BMP promotes motility and represses growth of smooth muscle cells by activation of tandem Wnt pathways

Vinicio A. de Jesus Perez,[1] Ziad Ali,[1] Tero-Pekka Alastalo,[2] Fumiaki Ikeno,[1] Hirofumi Sawada,[2] Ying-Ju Lai,[2] Thomas Kleisli,[2] Edda Spiekerkoetter,[1] Xiumei Qu,[1] Laura H. Rubinos,[4] Euan Ashley,[1] Manuel Amieva,[2] Shoukat Dedhar,[3] and Marlene Rabinovitch[2]

[1]Department of Medicine and [2]Department of Pediatrics, Stanford University, Stanford, CA 94305
[3]Department of Biochemistry and Molecular Biology, University of British Columbia, Vancouver, British Columbia V6T 1Z3, Canada
[4]Department of Pediatrics, Baylor College of Medicine, Houston, TX 77030

We present a novel cell-signaling paradigm in which bone morphogenetic protein 2 (BMP-2) consecutively and interdependently activates the wingless (Wnt)–β-catenin (βC) and Wnt–planar cell polarity (PCP) signaling pathways to facilitate vascular smooth muscle motility while simultaneously suppressing growth. We show that BMP-2, in a phospho-Akt–dependent manner, induces βC transcriptional activity to produce fibronectin, which then activates integrin-linked kinase 1 (ILK-1) via α4-integrins. ILK-1 then induces the Wnt–PCP pathway by binding a proline-rich motif in disheveled (Dvl) and consequently activating RhoA-Rac1–mediated motility. Transfection of a Dvl mutant that binds βC without activating RhoA-Rac1 not only prevents BMP-2–mediated vascular smooth muscle cell motility but promotes proliferation in association with persistent βC activity. Interfering with the Dvl-dependent Wnt–PCP activation in a murine stented aortic graft injury model promotes extensive neointima formation, as shown by optical coherence tomography and histopathology. We speculate that, in response to injury, factors that subvert BMP-2–mediated tandem activation of Wnt–βC and Wnt–PCP pathways contribute to obliterative vascular disease in both the systemic and pulmonary circulations.

Introduction

Chronic vascular disorders, such as atherosclerosis and pulmonary arterial hypertension (PAH; Humbert et al., 2004), are characterized by expansion of dedifferentiated cells bearing vascular smooth muscle cell (SMC [VSMC]) markers within the neointima and media of the vessel wall. The functional impact of this abnormality is that it increases resistance to blood flow and produces tissue ischemia (Raines and Ross, 1993; Willis et al., 2004). It has been proposed that, in response to vascular injury, proteolysis and subsequent alterations in the composition of the extracellular matrix induce the release and activation of mitogenic and motogenic factors that cause expansion, dedifferentiation, and migration of VSMCs (Chait, 1987; Voelkel and Tuder, 1997). For example, in the pulmonary circulation, endothelial injury can induce an elastolytic enzyme that both mediates release of growth factors (Goodall et al., 2001; Thompson and Rabinovitch, 1996) and enhances the potency of their biological effects by inducing tenascin-C–mediated activation of their receptors (Jones et al., 1997). Our recent studies have shown that signaling through the bone morphogenetic protein (BMP) receptor II (BMPRII) can both facilitate pulmonary artery (PA) SMC motility (Spiekerkoetter et al., 2009) and suppress proliferation in response to growth factors such as

Correspondence to Marlene Rabinovitch: marlener@stanford.edu

Abbreviations used in this paper: ANOVA, analysis of variance; AoSMC, aortic SMC; Apo, apolipoprotein; ARD, ankyrin repeat domain; βC, β-catenin; BMP, bone morphogenetic protein; BMPRII, BMP receptor II; Co-IP, coimmunoprecipitation; CSA, cross-sectional area; Dvl, disheveled; ERK, extracellular signal–related kinase; FN, fibronectin; ILK-1, integrin-linked kinase 1; IPAH, idiopathic PAH; OCT, optical coherence tomography; PA, pulmonary artery; PAEC, PA endothelial cell; PAH, pulmonary arterial hypertension; PCP, planar cell polarity; PRS, proline-rich sequence; ROCK I/II, Rho kinase I/II; SMC, smooth muscle cell; VSMC, vascular SMC; Wnt, wingless; WT, wild type.

The Rockefeller University Press $30.00
J. Cell Biol. Vol. 192 No. 1 171–188
www.jcb.org/cgi/doi/10.1083/jcb.201008060

PDGF-BB (Hansmann et al., 2008). In addition, other investigators have demonstrated that BMPRII ligands can reduce neointima formation in response to systemic vascular insults (Nakaoka et al., 1997).

Based on the aforementioned studies, it follows that neointima formation might occur in response to vascular damage in patients with dysfunctional BMPRII signaling. Although mutations in BMPRII are identified in 70% of patients with familial idiopathic PAH (IPAH) and 25% of those with sporadic IPAH, reduced BMPRII expression is noted in all forms of PAH (Machado et al., 2001; Humbert et al., 2004). Consistent with this, PASMCs isolated from IPAH patients carrying BMPRII mutations exhibit resistance to apoptosis and enhanced proliferation in response to growth factors (Morrell et al., 2001; Zhang et al., 2003).

In contrast to its role in the inhibition of proliferation, we recently showed that BMPRII-mediated signaling is necessary for PASMC motility (Spiekerkoetter et al., 2009). In human (h) PA endothelial cells (PAECs), BMPRII signals mediate motility by recruiting the noncanonical wingless (Wnt)–planar cell polarity (PCP) pathway via phospho (p) Smad interaction with disheveled (Dvl; de Jesus Perez et al., 2009). We therefore hypothesized that, in VSMCs, BMPRII-mediated signals might activate the Wnt–PCP pathway to facilitate cell motility while suppressing concurrent activation of the Wnt–β-catenin (βC) signaling pathway, which was shown to be pro-proliferative in hPAECs (de Jesus Perez et al., 2009).

Our results indicate that a novel tandem and interdependent activation of Wnt–βC and Wnt–PCP signaling is required for BMP-mediated VSMC motility. We show that BMP-2, via pAkt, inactivates GSK3β, causing transient accumulation and transcriptional activity of βC, which is required to increase production and secretion of fibronectin (FN). We show that FN interacts with α4-integrins to activate integrin-linked kinase 1 (ILK-1). This leads to the formation of a complex between ILK-1 and Dvl, which is necessary to both activate RhoA-Rac1–mediated VSMC motility and repress βC accumulation and VSMC proliferation. Using a murine aortic graft stent as an injury model, we show that transfection of a dominant-negative Dvl construct that causes persistent Wnt–βC activity without tandem recruitment of Wnt–PCP enhances neointima formation.

Results

BMP-2 stimulates PASMC migration via BMPRII-dependent activation of RhoA and Rac1

Previously, our group demonstrated that BMP-2 stimulates hPAEC motility via the Wnt–PCP pathway (de Jesus Perez et al., 2009). To investigate whether this mechanism was also involved in the regulation of motility in hPASMCs, we used a Boyden chamber assay. We demonstrated that 10 ng/ml BMP-2 increased hPASMC motility in a manner comparable with that observed with 20 ng/ml PDGF-BB, the positive control (Fig. 1 A). Next, we documented activation of the small GTPases RhoA and Rac1 (Fig. 1 B) using whole cell lysates harvested up to 6 h after stimulation with BMP-2. Active forms of RhoA and

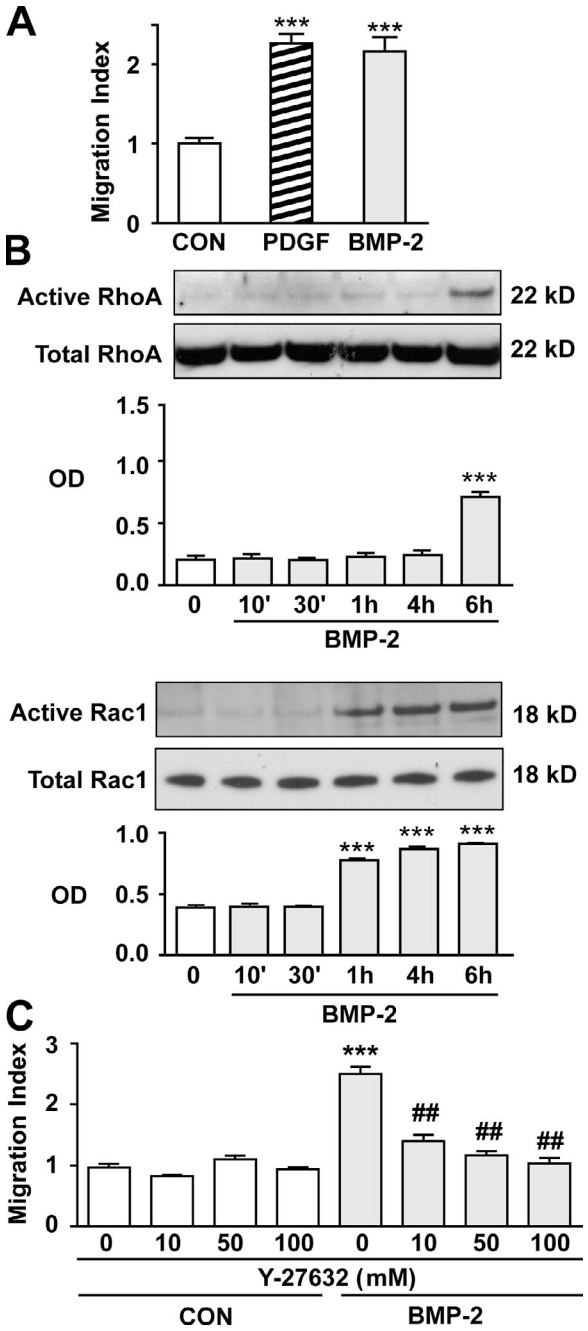

Figure 1. **BMP-2–mediated migration of hPASMCs requires activation of RhoA and Rac1.** (A) Migration was assessed using the Boyden chamber assay as described in Materials and methods. Cells were starved for 48 h in starvation media (0.1% FBS) before seeding them in Boyden chambers placed in 24-well plates containing either starvation media alone or supplemented with 10 ng/ml BMP-2 or 20 ng/ml PDGF-BB. (B) RhoA (top) and Rac1 (bottom) activation was measured in lysates from cells stimulated with BMP-2 over a period of 6 h using the approach described in Materials and methods. Densitometry values are shown relative to total RhoA and Rac1 in whole cell lysates that were run in different gels. (C) Motility response to BMP-2 was assessed in cells incubated with either Y-27632 at 10, 50, and 100 mM or DMSO for 6 h. Bars represent means ± SEM from $n = 3$ different cell harvests in triplicate. ***, $P < 0.0001$ versus control or time 0; and ##, $P < 0.001$ versus uninhibited control using one-way ANOVA with the Dunnett (A and B) or Bonferroni (C) tests. CON, control.

Rac1 were precipitated as described in Materials and methods. We found that, although BMP-2–mediated activation of Rac1 was observed at 1 h, an increase in active RhoA was evident only at 6 h (Fig. 1 B). To determine whether RhoA activation is required for BMP-2–induced PASMC migration, we blocked the activation of Rho kinase I/II (ROCK I/II), a downstream target of RhoA involved in cell motility. Indeed, using Y-27632, a specific ROCK I/II inhibitor (Loirand et al., 2006), we observed a dose-dependent reduction in BMP-2–mediated hPASMC migration (Fig. 1 C).

We next determined whether loss of function of BMPRII, previously shown to impair motility of cultured hPASMCs (Spiekerkoetter et al., 2009), does so by impeding activation of RhoA and Rac1. Using BMPRII siRNA (see Materials and methods), we confirmed reduced levels of BMPRII to <50% of control siRNA values 48 h after transfection, as previously reported by our group (Spiekerkoetter et al., 2009). This resulted in loss of RhoA and Rac1 activation in response to BMP-2 (Fig. S1 A). As expected, although BMP-2–mediated PASMC migration was lost in BMPRII-deficient cells, their response to PDGF-BB was preserved (Fig. S1 B).

BMP-2–mediated hPASMC migration requires the Wnt–βC pathway

We recently reported that BMP-2 simultaneously recruits the Wnt–βC pathway to induce proliferation of hPAECs and the Wnt–PCP pathway to stimulate migration (de Jesus Perez et al., 2009). Because BMP-2 does not mediate proliferation of hPASMCs (Morrell et al., 2001), we anticipated that the Wnt–βC pathway would not be activated. However, we found that BMP-2 induced a transient increase in βC beginning at 10 min, persisting for 4 h but falling below baseline levels at 6 h (Fig. 2 A). To investigate whether this transient increase in βC was required for BMP-2–mediated hPASMC migration, we transfected cells with two independent βC-specific siRNAs at a concentration that resulted in a >50% reduction in protein (Fig. S1 C) and performed Boyden chamber assays. In the setting of reduced βC, we not only found that BMP-2 failed to activate RhoA and Rac1 (Fig. 2 B) but also could not induce hPASMC migration (Fig. 2 C).

To determine whether the transient increase in βC after BMP-2 stimulation, which was required for hPASMC migration, was associated with βC transcriptional activity, we transfected cells with either the topflash βC reporter construct or fopflash, a mutated negative control (de Jesus Perez et al., 2009). A significant increase in reporter activity was found in hPASMCs stimulated with BMP-2 over a 6-h period (Fig. S1 E). Conversely, we confirmed that reduction of BMPRII was associated with loss of BMP-2–mediated βC transcriptional activity (Fig. S1 D). We next investigated how BMP-2 via BMPRII might be increasing βC accumulation and subsequent transcriptional activity.

BMP-2 increases βC levels in hPASMCs via pAkt-mediated disruption of the Axin–GSK3β–βC complex

Accumulation of βC levels in mammalian cells is largely dependent on disruption of binding between βC, Axin, and GSK3β (Ding et al., 2000; Logan and Nusse, 2004; Ng et al., 2009). Several kinases have been shown to participate in inducing βC accumulation by disrupting the βC–Axin–GSK3β degradation complex (Ding et al., 2005; Thornton et al., 2008). We have shown in PAECs that BMP-2 increases βC levels and transcriptional activity via p-extracellular signal related kinase (ERK)–mediated disruption of the βC–Axin–GSK3β degradation complex (de Jesus Perez et al., 2009). Based on this observation, we proposed that kinase-dependent disruption of the βC–Axin–GSK3β degradation complex was required for the BMP-2–mediated increase in βC. To test this, we determined whether βC accumulation could be temporally related to the phosphorylation state of kinases known to be activated by BMP stimulation, such as pERK, p-p38, and pAkt, in the setting of reduced BMPRII levels. We found that after 1 h of BMP-2 stimulation, activation of ERK and p38 but not Akt was evident in BMPRII-deficient hPASMCs (unpublished data). Furthermore, lack of Akt activation also associated with loss of GSK3β Ser 21 phosphorylation and βC accumulation. This led us to propose that pAkt could be regulating the stability of the βC–Axin–GSK3β degradation complex in hPASMCs.

To fully confirm the critical role of pAkt in regulating βC levels in hPASMCs, we transfected cells with either a vector or a dominant-negative (Δ) Akt construct (see Materials and methods). Consistent with our previous observations, we found that BMP-2 stimulation failed to induce βC accumulation and GSK3β Ser 21 phosphorylation in ΔAkt-transfected hPASMCs after 1 h (Fig. 3 A). Similar results were obtained when BMP-2 stimulation was repeated using hPASMC-incubated cells with 10 nM wortmannin, an inhibitor of Akt activation (García et al., 2009), for 1 h before addition of BMP-2. This abrogated phosphorylation of both Akt and GSK3β as well as βC accumulation (Fig. S2 A) and its transcriptional activity (Fig. S2 B), further supporting the requirement of Akt activation for BMP-2–mediated βC accumulation.

Because the pSmads 1/5/8 are also mediators of BMPRII signaling (Morrell, 2006) and regulate PAEC motility (de Jesus Perez et al., 2009), we investigated whether they might influence βC-dependent migration in hPASMCs. After transfection of a dominant-negative Smad 1 construct, we stimulated cells with BMP-2 and measured βC levels in whole cell lysates. We found that the BMP-2–induced increase in βC was not affected by disrupting pSmad 1 signaling (Fig. 3 B), suggesting that the mechanism for βC accumulation under BMP-2 stimulation is Smad 1/5/8 independent.

BMP-2 requires βC to induce FN in hPASMCs

Our next goal was to identify targets of BMP-2–mediated βC accumulation and transcriptional activity that could be related to hPASMC motility. FN is dependent on Wnt–βC signaling during murine lung development (De Langhe et al., 2005) and has also been implicated in VSMC motility (Boudreau et al., 1991). Our study shows that BMP-2 induced a greater than twofold increase in FN mRNA, peaking as early as 1 h after stimulation and remaining elevated over control levels at 4 h (Fig. 4 A). Furthermore, an increase in secreted FN was also noted as early

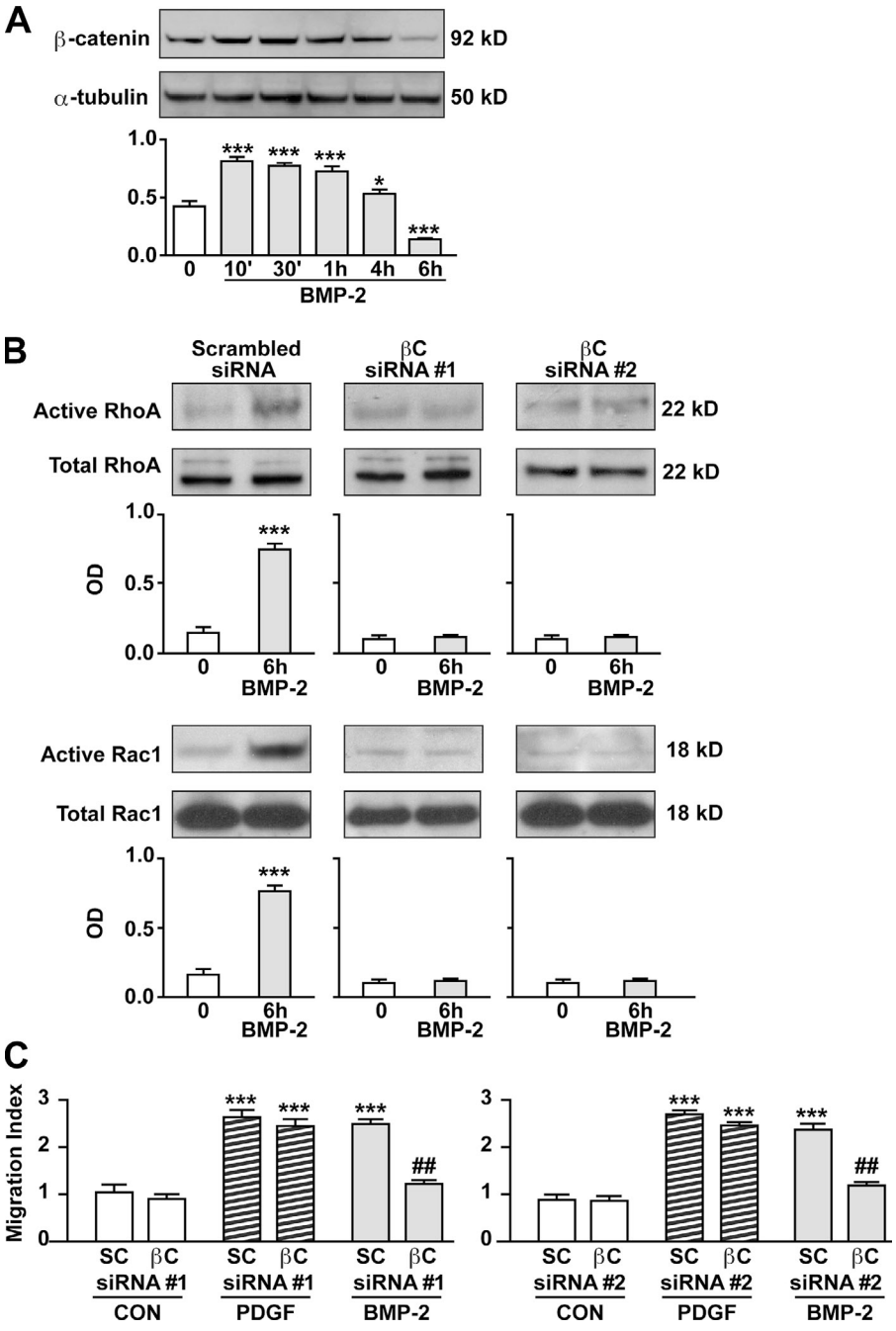

Figure 2. **Activation of βC is required for BMP-2–mediated hPASMC motility.** (A) Levels of active βC in lysates obtained from 10 ng/ml BMP-2–stimulated cells over 6 h were measured by Western immunoblotting (top) and quantified using densitometry (bottom) expressed as the ratio of the OD of βC relative to α-tubulin. (B) RhoA (top) and Rac1 (bottom) activation was measured in lysates from cells transfected with either scrambled or two independent βC siRNAs stimulated with BMP-2 over a period of 6 h using the approach described in Materials and methods. Densitometry values are shown relative to total RhoA and Rac1 in whole cell lysates, which were run in different gels. (C) Boyden chamber assays were performed as previously described to measure the impact of two independent βC versus scrambled (SC) siRNA on hPASMC motility. Bars represent means ± SEM from $n = 3$. *, $P < 0.01$; and ***, $P < 0.0001$ versus control (CON) in A and B were determined using one-way ANOVA with Dunnett's. ***, $P < 0.0001$ versus time 0; and ##, $P < 0.001$ versus scrambled siRNA in C were determined using one-way ANOVA with Bonferroni's.

as 1 h and remained elevated at 4 and 6 h after BMP-2 stimulation (Fig. 4 B). The BMP-2–mediated increase in FN was βC dependent, as it was lost in cells treated with two independent βC-specific siRNAs but not control siRNA (Fig. 4 B). Immunofluorescence staining of hPASMCs showed an increase in FN as early as 1 h after BMP-2 stimulation, which was lost when cells were pretreated with βC siRNA (Fig. 4 C).

ILK-1 activation is required for BMP-2–mediated hPASMC motility

FN directs cell movement through its interaction with integrin receptors located on cell surfaces (Troussard et al., 1999) and by subsequent activation of ILK-1 (Legate et al., 2009; Streuli and Akhtar, 2009; Vicente-Manzanares et al., 2009). To determine whether BMP-2 could activate ILK-1 in an FN-dependent manner, ILK-1 kinase activity was first measured by incubating lysates from BMP-2–stimulated cells with GSK3β, a known substrate of ILK-1, followed by measurement of Ser 21 phosphorylation. BMP-2 induced significantly higher levels of ILK-1 activity at 1 and 4 h after stimulation when compared with baseline (Fig. 5 A). When cells were incubated with 5 µg/ml CS-1, an FN-specific peptide that interacts with the α4β1-integrin complex and prevents its binding to FN, no ILK-1 activity was observed. Furthermore, coincubation with CS-1 selectively abrogated BMP-2–mediated PASMC migration (Fig. 5 B). Because CS-1 is highly specific for the α4β1-integrin receptor complex (Waitkus-Edwards et al., 2002), our findings suggest that binding of FN to the

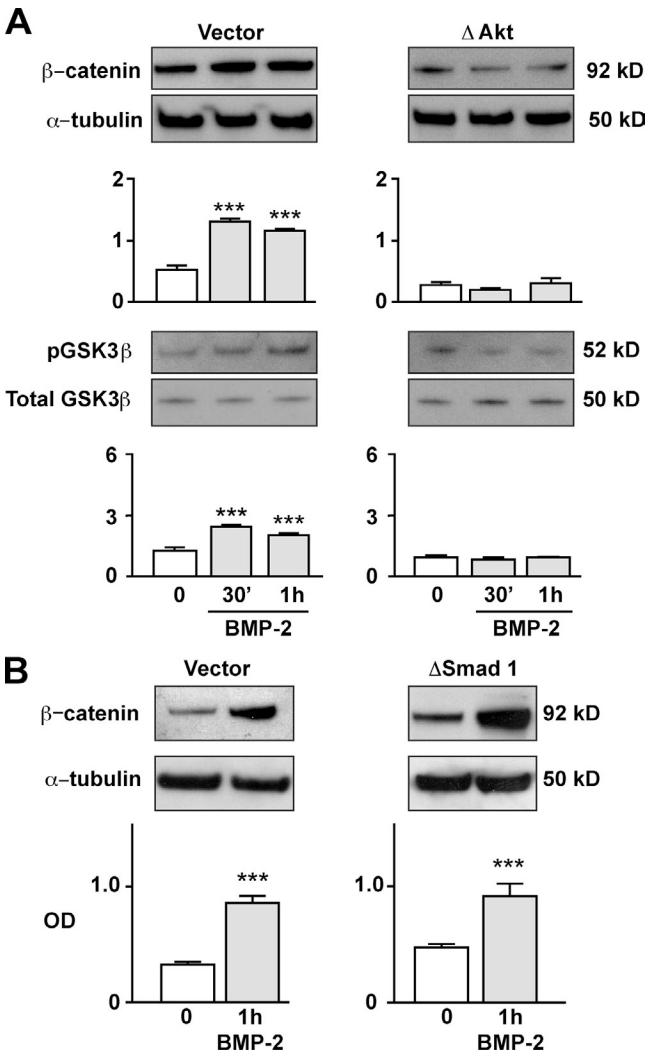

Figure 3. **BMP-2 activates βC via pAkt-dependent inhibition of GSK3β and is independent of Smad signaling.** (A and B) βC activation in 10 ng/ml BMP-2–stimulated hPASMCs transfected with a nonfunctional pAkt (ΔAkt) in A and a Smad 1 construct (ΔSmad 1) in B was measured by immunoblot analysis and compared with values in cells transfected with vector alone. The pGSK3β activation in A was measured relative to total GSK3β. Bars represent means ± SEM from $n = 3$. ***, $P < 0.0001$ versus time 0 in A was determined using one-way ANOVA with Dunnett's. ***, $P < 0.0001$ in B were determined using the unpaired t test.

α4β1 is required for BMP-2–mediated activation of ILK-1 and PASMC motility.

We next investigated whether ILK-1 is required for migration of hPASMCs in response to BMP-2 stimulation. To test this, we transfected cells with either scrambled or ILK-1 siRNA to produce a >50% knockdown in ILK-1 protein levels (Fig. S2 C) and studied the motility response to BMP-2 using the Boyden chamber assay. ILK-1–deficient hPASMCs failed to migrate in response to BMP-2, but the response to PDGF-BB was unchanged (Fig. 5 C). When levels of active RhoA and Rac1 were measured in cell lysates using the pull-down assay as reported earlier in this paper, we also found that ILK-1–deficient cells lacked RhoA and Rac1 activation in response to stimulation with BMP-2 (Fig. 5 D).

Collectively, these experiments support a requirement for ILK-1 in modulating the migratory response of hPASMCs to BMP-2. Although various studies have shown that ILK-1 can regulate the activity of the Wnt–βC pathway (Dwivedi et al., 2008; Ho and Bendeck, 2009), evidence for a similar role in the regulation of the Wnt–PCP pathway is lacking. However, this possibility is reinforced by a previous study documenting an interaction between ILK-1 and Dvl in renal epithelial cells (Torres and Nelson, 2000). Dvl is a necessary intermediate in the signaling of both the canonical and noncanonical Wnt pathways (Boutros et al., 1998; Logan and Nusse, 2004). In fact, our previous work in hPAECs revealed that BMP-2 induces migration via a Dvl-dependent activation of downstream components of the Wnt–PCP pathway, i.e., RhoA and Rac1 (de Jesus Perez et al., 2009).

Interaction between ILK-1 and Dvl regulates hPASMC motility

The next goal of our experiments was to show that BMP-2 could affect Dvl distribution in hPASMCs and induce a physical interaction between Dvl and ILK-1, which is necessary to activate RhoA and Rac1 and to mediate hPASMC motility. To confirm that translocation of Dvl to the periphery and leading edges is required for BMP-2–induced hPASMC migration, cells transfected with wild-type (WT) Dvl-GFP constructs were seeded in borosilicate sterile dual-chamber slides, and cell movement was followed over 10 h using time-lapse fluorescent video microscopy (see Materials and methods). Compared with unstimulated controls, BMP-2–stimulated cells formed GFP-rich lamellipodiae and covered a greater physical distance (Videos 1 and 2), whereas cells transfected with the ΔDEP Dvl construct failed to respond to BMP-2 (Videos 3 and 4). Finally, to establish that Dvl and ILK-1 can interact in hPASMCs under BMP-2 stimulation, we looked at the distribution of ILK-1 and Dvl by transfecting fluorophore-tagged constructs into hPASMCs. Cotransfection of V5-tagged WT ILK-1 and GFP-tagged Dvl constructs revealed colocalization of the ILK-1 and Dvl signals when assessed by confocal microscopy as early as 1 h after BMP-2 stimulation (Fig. 6 A).

We next sought to characterize which sector of the Dvl structure is involved in establishing contact with ILK-1 during the BMP-2–mediated complex formation. It has been previously shown that Dvl-mediated activation of the Wnt–βC or the Wnt–PCP signaling pathway is dependent on the availability of the specific Dvl domains DIX, PDZ, and DEP (Axelrod et al., 1998; Boutros et al., 1998). Although DIX is mainly involved in Wnt–βC signaling, PDZ and DEP appear to be required in Wnt–PCP functions, with PDZ affecting RhoA and DEP linked to Rac1 activation (Axelrod et al., 1998; Boutros et al., 1998). In addition, analysis of the secondary and tertiary structure of the ILK-1 protein has shown that, in addition to the kinase domain at the C terminus, there is an ankyrin repeat domain (ARD) at the N terminus (Velyvis et al., 2001). The ARD is a common protein–protein interaction motif that allows ILK-1 to interact with a wide variety of proteins in various cellular compartments (Dobreva et al., 2008), especially with those such as PINCH-1, which are involved in cytoskeletal regulation and cell motility (Zhang et al., 2002; Fukuda et al., 2003). In addition, the Frizzled receptors use ARDs to regulate the activity

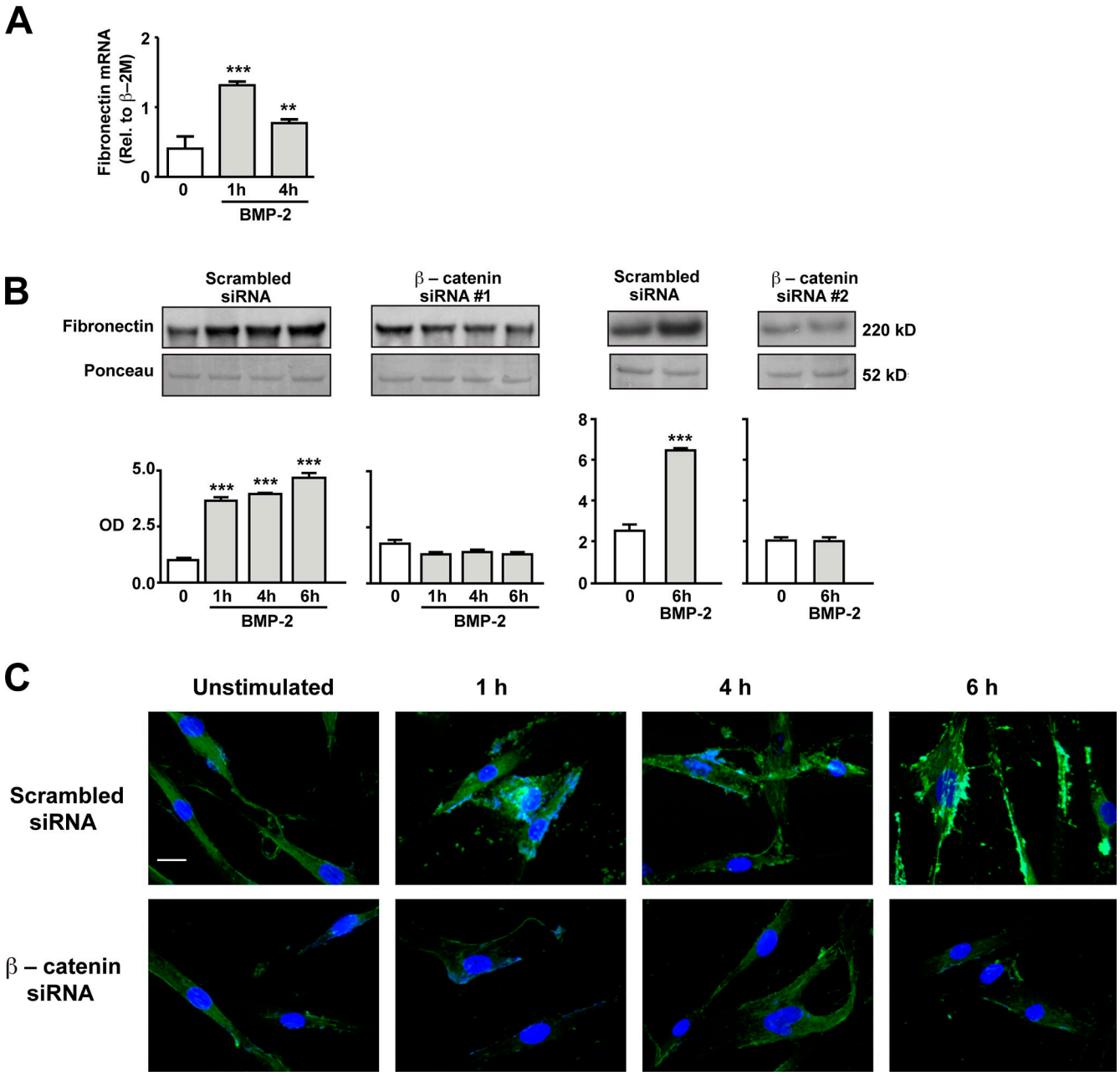

Figure 4. **Production and secretion of FN is dependent on BMP-2–mediated activation of βC.** (A and B) Quantitative RT-PCR (A) and Western immunoblotting (B) were used to measure changes in levels of FN mRNA and protein, respectively, in hPASMCs stimulated with 10 ng/ml BMP-2 over a period of 6 h. In B, levels of secreted FN were measured in hPASMCs transfected with either scrambled or two independent βC siRNAs. Densitometry values were expressed as the ratio of OD of FN relative to the Ponceau stain of an unrelated band in media samples concentrated by ultrafiltration. Bars represent means ± SEM from $n = 3$. **, $P < 0.001$; and ***, $P < 0.0001$ versus time 0 using one-way ANOVA with Dunnett's. (C) Representative immunofluorescence images showing FN distribution in scrambled (top) or βC siRNA (bottom)–transfected hPASMCs stimulated with 10 ng/ml BMP-2 over 6 h. DAPI (blue) stain was used to label cell nuclei. Bar, 10 µm.

of some components of the Wnt–PCP pathway (Feiguin et al., 2001; Das et al., 2004). Analysis of Dvl mutants in *Drosophila melanogaster* revealed that mutations in the region between the PDZ and DEP domains (amino acids 312–362) contain a proline-rich sequence (PRS) that could act as a putative SH3-binding domain and assist in protein–protein interactions (Penton et al., 2002). Furthermore, in addition to its role as an SH3-binding domain, the PRS also serves as a binding platform for ARD in proteins such as ANKRA (Rader et al., 2000). Review of the sequence of each of our Dvl constructs showed a preservation of the PRS, leading us to postulate that, whereas binding to PRS in the context of an intact PDZ may be necessary for initial ILK-1–Dvl interaction, stabilization after BMP-2 stimulation requires that the PRS domain be presented in a conformation that also involves the DEP domain.

To map the site of the Dvl–ILK-1 interaction, we used two previously described GFP-tagged Dvl constructs: one containing a WT form and another (ΔDEP Dvl) containing a truncated

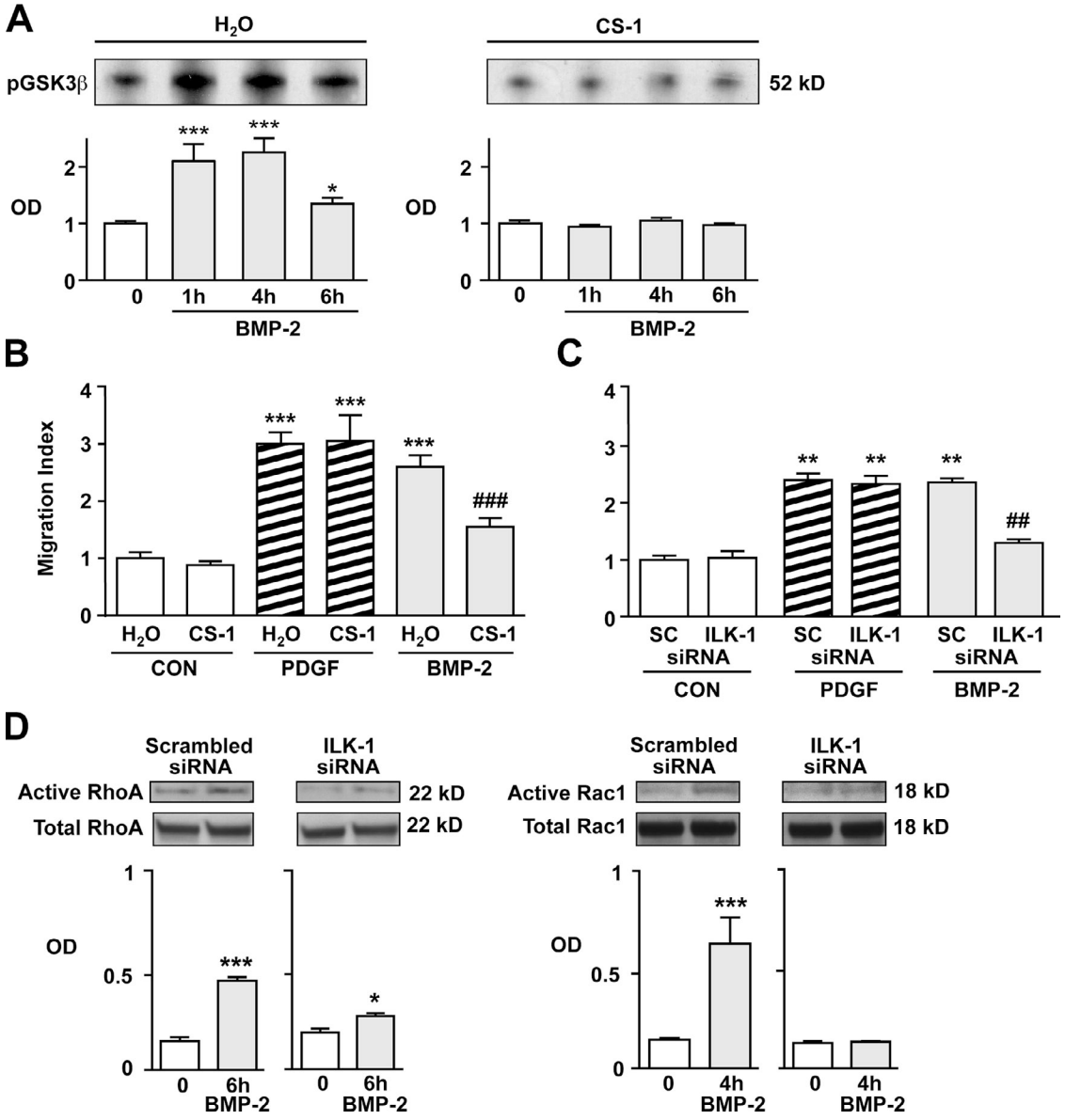

Figure 5. **Activation of integrin-linked kinase 1 (ILK-1) is required for BMP-2–mediated hPASMC motility.** (A) ILK-1 kinase assay was performed as described in Materials and methods with GSK3β as the substrate on cells incubated in the presence (right) or absence (left) of 5 µg/ml CS-1. (B and C) Motility in hPASMCs exposed to CS-1 (B) or transfected with either scrambled (SC) or ILK-1–specific siRNA (C) and exposed to 10 ng/ml BMP-2 was measured using the Boyden assay. (D) Levels of active RhoA and Rac1 were measured as described in Materials and methods. Densitometry values are shown relative to total RhoA and Rac1 in whole cell lysates, which were run in different gels. Bars represent means ± SEM from $n = 3$. In A, *, $P < 0.01$; and ***, $P < 0.0001$ were determined using one-way ANOVA with Dunnett's. In B and C, **, $P < 0.001$; and ***, $P < 0.001$ versus baseline; and ##, $P < 0.001$; and ###, $P < 0.0001$ versus respective scrambled siRNA control using one-way ANOVA with Bonferroni's. In D, *, $P < 0.01$; and ***, $P < 0.0001$ versus time 0 were determined using an unpaired *t* test. CON, control.

version lacking the DEP (i.e., Rac1 activating) domain (Axelrod et al., 1998; de Jesus Perez et al., 2009). In addition, we used the WT Dvl construct to generate a mutant containing functional DIX, PDZ, and DEP domains and a nonfunctional PRS (see Materials and methods). These constructs were then transfected into hPASMCs, and their ability to bind to ILK-1 was measured using coimmunoprecipitation (Co-IP; see Materials and methods). In contrast to the temporal increase in Dvl–ILK-1 complex formation seen in BMP-2–stimulated hPASMCs transfected with WT Dvl, unstimulated cells transfected with ΔDEP Dvl showed increased complex formation that fell below baseline levels under BMP stimulation, whereas those transfected with ΔPRS Dvl failed to form ILK-1–Dvl complexes either at baseline or upon BMP-2 stimulation (Fig. 6 B). Despite their differences in the patterns of Dvl–ILK-1 complex formation, both ΔDEP and ΔPRS Dvl–transfected cells failed to activate RhoA-Rac1 (Fig. 6 C) or migrate in response to BMP-2 when compared with cells transfected with WT Dvl (Fig. 6 D).

The presence of ΔDEP Dvl facilitates proliferation in response to PDGF-BB

Besides its role in promoting RhoA and Rac1 activation, the recruitment of Dvl by ILK-1 may also shuttle Dvl away from the Wnt–βC pathway, leading to enhanced GSK3β activity and

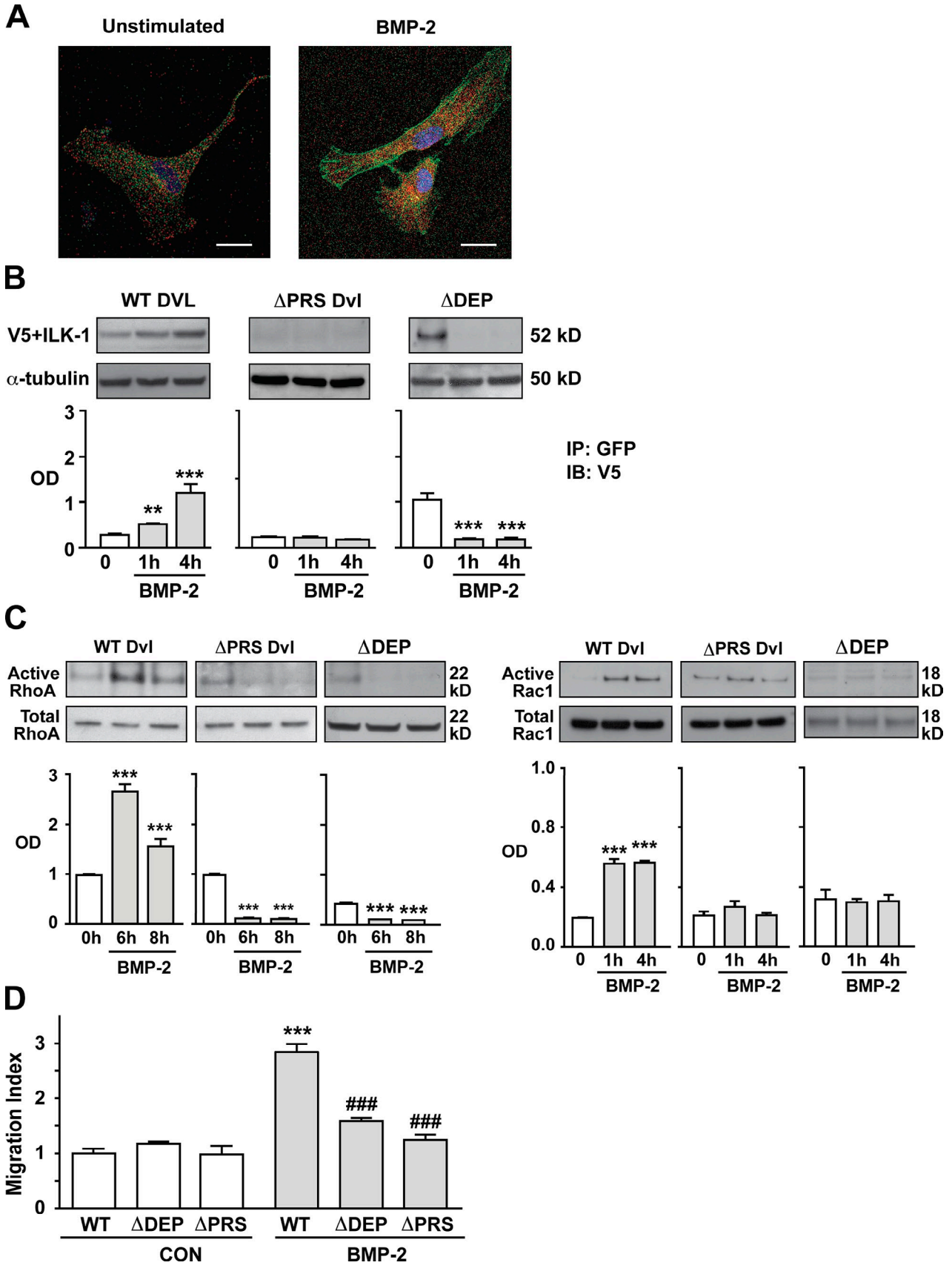

Figure 6. **ILK-1–dependent recruitment of Dvl is necessary for BMP-2–mediated hPASMC migration.** (A) Confocal microscopy was used to localize ILK-1 (red) and Dvl (green) in hPASMCs stimulated with 10 ng/ml BMP-2. DAPI (blue) was used to label the nuclei. Bars, 10 µm. (B) Co-IP of V5-tagged ILK-1 and WT, ΔDEP, and ΔPRS Dvl-GFP constructs under 10 ng/ml BMP-2 stimulation. Levels of V5-tagged ILK-1 were measured against levels of α-tubulin in whole

reduction in βC levels (Logan and Nusse, 2004). This could explain the significant decrease in βC below baseline levels seen 6 h after BMP stimulation (Fig. 2 A) and could be linked to the reduction in PASMC proliferation documented with BMP stimulation (Zhang et al., 2003; Hansmann et al., 2008). To assess the possibility that disrupting Wnt–PCP in hPASMCs increases βC levels, we transfected cells with WT or ΔDEP Dvl-GFP and stimulated them with 10 ng/ml BMP-2 for 6 h. We used ΔDEP rather than the ΔPRS Dvl construct because we had previously shown that this construct fails to bind to activated ILK-1 after BMP-2 stimulation. We hypothesized that suppression of Wnt–PCP activation by ΔDEP Dvl would result in sustained βC protein levels and transcriptional activity in cells stimulated with BMP-2. Indeed, we were able to show that in ΔDEP Dvl–transfected PASMC, both βC and pGSK3β levels remained elevated at 6 h after BMP-2 stimulation, whereas in cells transfected with WT Dvl, pGSK3β and βC values were below baseline at that time point (Fig. 7 A, left and middle). To explain the persistent elevation of βC in ΔDEP-transfected hPASMCs, we postulated that the inability of Dvl to bind to ILK-1 under BMP-2 stimulation would allow more Dvl to remain bound to GSK3β, thereby preventing its ability to phosphorylate and target βC for proteasomal degradation (Logan and Nusse, 2004). To test this, we performed Co-IP experiments in cells transfected with either WT or ΔDEP Dvl and measured the association between pGSK3β and the two Dvl constructs over 6 h after BMP-2 stimulation. Our findings demonstrate that, although pGSK3β–Dvl complexes in WT Dvl–transfected cells appear at 1 h and fall by 6 h, formation of the complex persists at 6 h in the ΔDEP Dvl–transfected hPASMCs (Fig. 7 A, right).

We then investigated whether persistent elevation in βC activity could subvert the antiproliferative effects of BMPs in ΔDEP Dvl–transfected hPASMCs when exposed to growth factors. To test this, we transfected cells with either WT or ΔDEP Dvl and exposed them with PDGF-BB, BMP-2, or both for 72 h and measured changes in cell numbers. We found that PDGF-BB–mediated proliferation of hPASMCs was augmented in ΔDEP Dvl compared with the WT Dvl–transfected cells (Fig. 7 B). Moreover, BMP-2 suppressed the PDGF-BB–mediated growth response in WT Dvl but not in ΔDEP Dvl–transfected hPASMCs. Cotransfection of hPASMCs with ΔDEP or WT Dvl, along with either scrambled or two independent βC-specific siRNA, was performed (Fig. 7 C, top and bottom). We found that knockdown of βC reduced PDGF-BB–mediated proliferation in both WT and ΔDEP Dvl hPASMCs and abrogated the enhanced growth response to PDGF-BB observed previously in ΔDEP Dvl–transfected hPASMCs (Fig. 7 C, top and bottom). In addition, we found that BMP-2–mediated suppression of PDGF-BB was partially restored in hPASMCs transfected with ΔDEP Dvl and two independent βC siRNAs.

Transfection of a constitutively active βC construct promotes hPASMC motility and proliferation

Our study has shown that temporal regulation of βC levels by BMP-2 is essential to prevent hPASMC proliferation. Based on the data provided by the aforementioned studies, we proposed that constitutive activation of βC would increase both proliferation and motility of hPASMCs independent of BMP-2 stimulation. To test this, we transfected hPASMCs with either an empty vector or a plasmid containing a mutated version of βC (gift from W. J. Nelson, Stanford University, Stanford, CA) lacking the N-terminal phosphorylation sites (ΔβC), making it resistant to proteasomal degradation (see Materials and methods). We found that ΔβC-transfected cells had higher baseline levels of activated RhoA-Rac1 (Fig. 8 A), with an associated increase in FN production (Fig. 8 B) and motility (Fig. 8 C) compared with vector-transfected cells. Finally, cell count studies of ΔβC-transfected cells also confirmed that their proliferation is significantly higher than that of their corresponding controls (Fig. 8 D).

In conclusion, we found that a constitutive increase in βC levels, independent of BMP-2 stimulation, can trigger an increase in both hPASMC motility and proliferation. This stresses the critical need for a functional BMP-signaling pathway to properly regulate βC levels and preserve the balance between proliferation and motility, which is especially important in the response to vascular injury.

Transfection of ΔDEP leads to severe intimal thickening in stented aortic grafts

As our experiments showed that recruitment of Dvl by ILK-1 is necessary to initiate BMP-mediated motility in cultured hPASMCs and to suppress growth factor–mediated proliferation, we investigated whether these features were also applicable to systemic arterial SMCs and to neointima formation in pulmonary or systemic vascular disease (Willette et al., 1999). We showed that human aortic SMCs (AoSMCs) stimulated with BMP-2, such as hPASMCs, displayed an initial early rise in βC followed by a fall below baseline levels starting at 4 h (Fig. S3 A). Consistent with the response in hPASMCs, hAoSMCs transfected with WT Dvl migrated in response to BMP-2 but not when transfected with ΔDEP Dvl (Fig. S3 B).

We next investigated the impact of interfering with BMP-mediated Wnt–PCP-induced motility and suppression of proliferation in the intact animal. Because murine models of PA neointima formation require a long time, and not all peripheral arteries show the lesions (Spiekerkoetter et al., 2009), we used the murine aortic stent model. A segment from the abdominal aorta of C57BL/6J was treated with balloon dilation and insertion of a metal stent to induce endovascular injury (see Materials and methods for details; Ali et al., 2007). Before grafting into the internal carotid artery, aortic segments were sonoporated to

cell lysates analyzed in a separate gel. (C) RhoA (left) and Rac1 (right) activation in BMP-2–stimulated hPASMCs transfected with either WT, ΔDEP, or ΔPRS Dvl was performed as described in Materials and methods. Levels of active RhoA and Rac1 were measured against levels of total RhoA and Rac1 in whole cell lysates analyzed in a separate gel. (D) Boyden chamber assays were performed as previously described to measure the impact of WT, ΔDEP, and ΔPRS Dvl on BMP-2–induced hPASMC motility. Bars represent means ± SEM from $n = 3$. **, $P < 0.001$; and ***, $P < 0.0001$ versus time 0 in B and C using one-way ANOVA with Dunnett's. ***, $P < 0.0001$ versus control (CON) unstimulated; and ###, $P < 0.0001$ versus WT stimulation in D was determined using one-way ANOVA with Bonferroni's. IP, immunoprecipitation. IB, immunoblot.

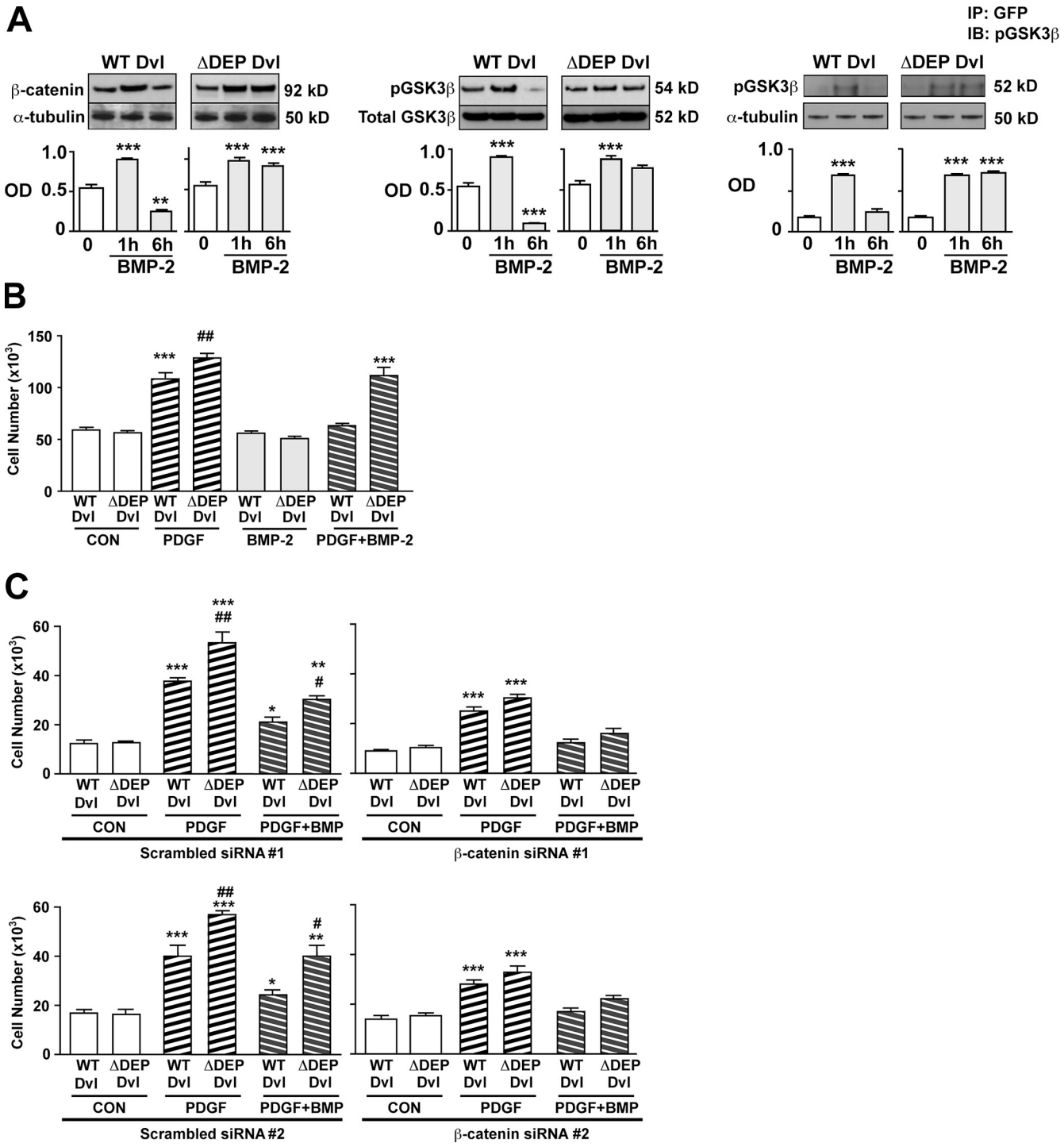

Figure 7. **Presence of ΔDEP Dvl promotes VSMC growth response to PDGF-BB by increasing βC levels.** (A) Levels of active βC (left) and pGSK3β (middle) in hPASMCs transfected with either WT or ΔDEP Dvl and stimulated with 10 ng/ml BMP-2 were visualized by Western immunoblotting and quantified by densitometry. Levels of active βC were normalized to α-tubulin, and levels of pGSK3β were normalized to total GSK3β in whole cell lysates. Co-IP of pGSK3β and WT and ΔDEP (right) was carried under BMP-2 stimulation. Levels of pGSK3β were normalized relative to total GSK3β in whole cell lysates analyzed in a separate gel. (B) Cell count studies were performed after addition of PDGF-BB, BMP-2, or both for 72 h. (C) Cell count studies were performed in hPASMCs cotransfected with WT or ΔDEP Dvl and either scrambled or two independent βC siRNAs after addition of PDGF-BB, BMP-2, or both for 72 h. **, $P < 0.001$; and ***, $P < 0.0001$ as indicated in A were determined by one-way ANOVA with Dunnett's. Bars represent mean ± SEM from $n = 3$. *, $P < 0.01$; **, $P < 0.001$; and ***, $P < 0.0001$ versus baseline; #, $P < 0.01$; and ##, $P < 0.001$ versus scrambled counterpart as indicated in B and C using one-way ANOVA with Bonferroni's. CON, control; IP, immunoprecipitation. IB, immunoblot.

introduce either WT or ΔDEP Dvl-GFP constructs throughout the vessel wall. Transfection efficiency after sonoporation was confirmed via immunohistochemistry (Fig. S3 C). Our results using both quantitative optical coherence tomography (OCT; Fig. 9 A) and histomorphometry (Fig. 9 B) of vessel sections revealed that the neointima area was more than twofold increased

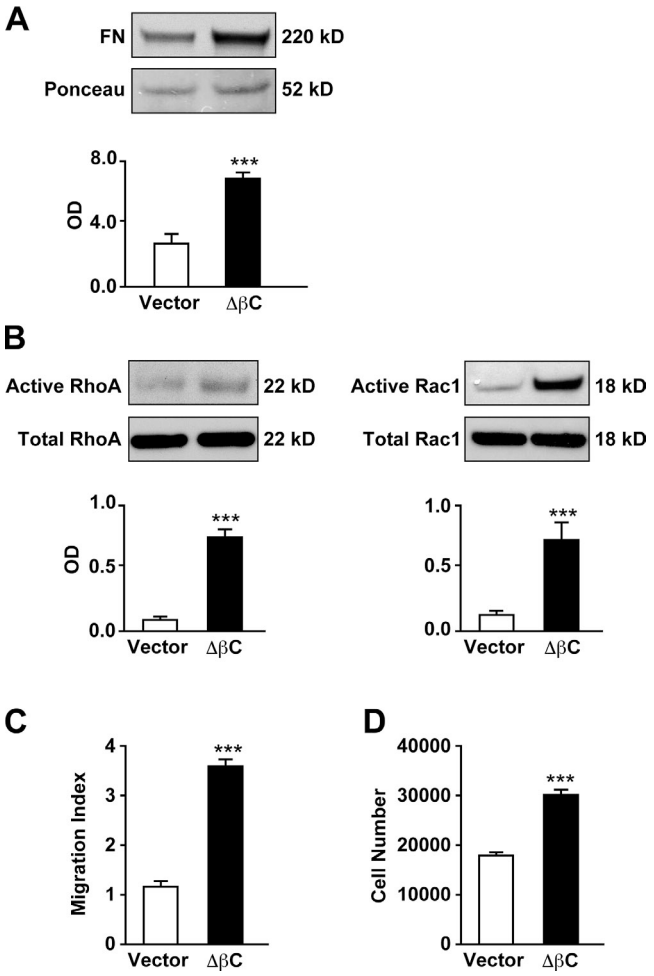

Figure 8. **Constitutively active βC induces FN production, RhoA-Rac1, motility, and proliferation in hPASMCs.** (A) Levels of secreted FN were measured in hPASMCs transfected with either vector or ΔβC. Densitometry values were expressed as the ratio of OD of FN relative to the Ponceau stain of an unrelated band in media samples concentrated by ultrafiltration. (B) RhoA (left) and Rac1 (right) activation in BMP-2–stimulated hPASMCs transfected with either vector or ΔβC was performed as described in Materials and methods. Levels of active RhoA and Rac1 were measured against levels of total RhoA and Rac1 in whole cell lysates analyzed in a separate gel. (C) Boyden chamber assays were performed as previously described in this paper to measure the impact of vector or ΔβC on hPASMC motility. (D) Cell count studies in hPASMCs transfected with either vector or ΔβC were performed for 72 h. Bars represent means ± SEM from $n = 3$. ***, $P < 0.0001$ versus vector using an unpaired t test.

in ΔDEP Dvl–treated vessels compared with WT Dvl, whereas the lumen area was decreased. Stent expansion was not different between groups. None of the cross-sectional images obtained with OCT showed evidence of thrombi. DAPI staining of graft cross sections revealed that the neointima was comprised of many cells in ΔDEP compared with WT Dvl–transfected vessels (Fig. 9 C), supporting a heightened proliferative response.

Discussion

Using isolated hPASMCs and a murine model of vascular injury, we show, for the first time to our knowledge, that BMP signaling can induce tandem recruitment of the Wnt–βC and the Wnt–PCP pathways to induce motility (Fig. 10 A) and suppress proliferation of SMCs (Fig. 10 B), thereby regulating their contribution to vascular remodeling after vascular injury.

Previous work by our group has demonstrated that BMP-2 promotes hPAEC motility by activating RhoA and Rac1 signaling in a Dvl-dependent fashion, concluding that recruitment of Wnt–PCP is necessary for induction of cell motility (de Jesus Perez et al., 2009). Although our current study confirms that BMP-2 also regulates SMC motility through a Dvl-dependent Wnt–PCP pathway, the process takes longer because it requires βC-mediated FN production. Also, BMP-2 activation of Rac1 precedes that of RhoA, whereas they occur simultaneously in response to BMP-2 in hPAECs. As BMP-2–induced activation of RhoA and Rac1 in hPASMCs is modulated by FN-mediated ILK-1 binding to Dvl, it is possible that the conformational change in Dvl after this interaction allows preferential exposure of the DEP domain, thereby facilitating its earlier activation. Later activation of RhoA may be caused by a change in the composition of the protein complex, possibly from involvement of other binding partners that allow the PDZ domain to be properly exposed. A similar pattern of delayed RhoA relative to Rac1 activation has been shown in neurons in response to netrin-1 and appears necessary to coordinate the relocalization of cytoskeletal and molecular elements required for axonal extension during cell growth (Picard et al., 2009). Among possible molecules that bind to the ILK-1–Dvl complex is the scaffolding protein chloride intracellular channel 4, which we have previously identified as a necessary component of BMP-2–mediated hPASMC motility (Spiekerkoetter et al., 2009). In addition, it is interesting that we also previously reported that apolipoprotein (Apo) D stimulates SMC motility in a manner that synergizes with PDGF-BB in activating Rac1 (Leung et al., 2004), but ApoD also suppresses PDGF-BB–mediated SMC proliferation by preventing nuclear translocation of pERK (Sarjeant et al., 2003).

In contrast to hPAECs in which BMPRII-dependent pERK activation is required for GSK3β inhibition, BMP-2 selectively recruits pAkt in hPASMCs to inactivate the GSK3β–Axin–βC degradation complex. After binding BMP-2, physical interaction between BMPRII and Akt may be facilitated in hPAECs because studies have shown these proteins are clustered within caveolae (Sedding et al., 2005; Wertz and Bauer, 2008). In contrast, in hPASMCs, BMP-2–mediated pERK is dependent not on BMPRII but on the receptor for end products of glycation, as shown previously by our group (Spiekerkoetter et al., 2009).

The pAkt-mediated βC activation in hPASMCs is transient, and the fall in βC is linked both temporally and functionally to ILK-1 binding to Dvl. This would suggest that Dvl is required in the Wnt–βC pathway to facilitate or sustain the inhibition of GSK3β, the main regulator of βC levels in mammalian cells. This model is consistent with the concept that, in binding Dvl, ILK-1 restores the stability of the GSK3β–Axin–βC complex, which is required to target βC for proteasomal degradation (Fig. 10 A). This mechanism would appear necessary to prevent βC accumulation, which, as is evident in our study, can derepress cell proliferation in response to growth factors. Conversely, the inability of mutant Dvl to bind ILK-1 may allow ILK-1 to inactivate its substrate GSK3β (Troussard et al., 1999),

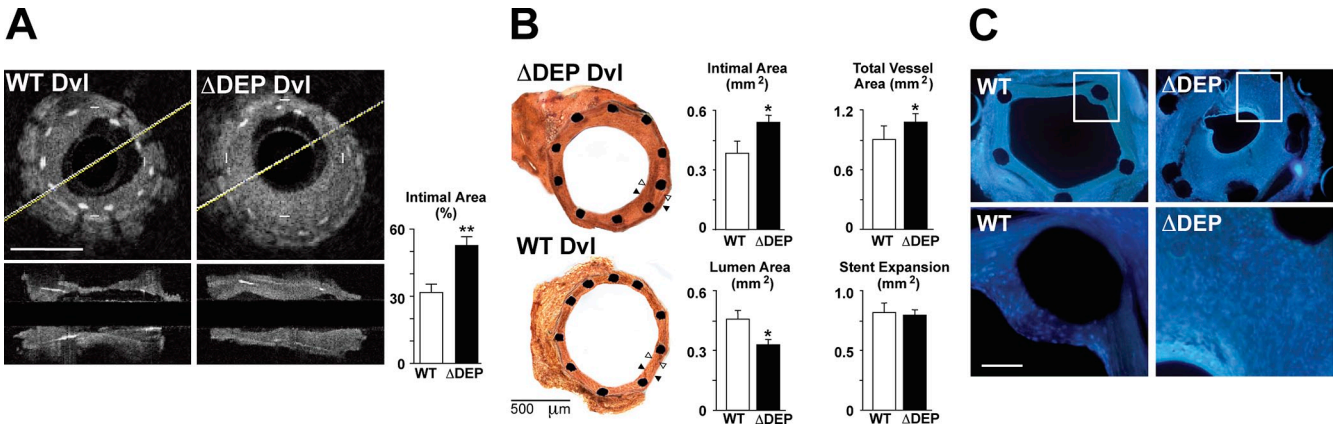

Figure 9. **Transfection of ΔDEP leads to increased neointima thickening in stented aortic grafts.** Thoracic aortas from C57BL/6J mice were cannulated with a balloon angioplasty catheter and inflated to eight atmospheres for 30 s followed by insertion of a 2.5 × 6–mm metal stent as described in Materials and methods. (A) OCT cross-sectional (top) and longitudinal (bottom) images of the grafts transfected with WT (left) and ΔDEP (right) Dvl were obtained, and intimal thickening was quantified. Values are expressed as percentages of the intimal area measured by comparing the cross-sectional area of the intima relative to the cross sectional area of the stent. The cross-sectional area of the intima is measured as the region above the white stent struts that protrude into the lumen. Yellow lines identify the center of the source for the infrared light in the OCT catheter. Bar, 200 μm. (B) Intimal response to balloon angioplasty and stenting comparing WT Dvl or ΔDEP Dvl. Representative images of histological sections at low power from each group are shown. In both images, black arrowheads denote the vessel wall (endothelium to external elastic lamina), and white arrowheads show the neointima (subendothelial space to internal elastic lamina). Note that in the region illustrated by the arrowheads there is a very small distance between the fragmented internal elastic and the external elastic laminae. An unpaired *t* test was used to show the difference between WT and ΔDEP Dvl; *, $P < 0.05$; and **, $P < 0.001$ ($n = 5$–6 mice per group). (C) Cross-sectional images of WT (left) and ΔDEP (right) Dvl–transfected grafts stained with DAPI. Insets in the top images represent the areas illustrated on the bottom. Bar, 100 μm.

leading to a persistent accumulation of βC (Fig. 10 B). In contrast to these findings in hPASMCs, the simultaneous activation of Wnt–βC and Wnt–PCP pathways in hPAECs suggests the availability of two separate pools of Dvl.

Our study has identified BMP-2–mediated FN production as the bridge connecting Wnt–βC with the Wnt–PCP signaling in hPASMCs. Although various groups have already shown that BMP-2 can induce production and release of FN in mesenchymal precursor cells and osteoblasts through recruitment of Runx2 (Lee et al., 2000), we show, for the first time to our knowledge, that in SMCs, this process is regulated by βC. This is in keeping with previous observations that link Wnt–βC signaling to the regulation of FN production during lung development (De Langhe et al., 2005) as well as in diseases such as renal and pulmonary fibrosis (Königshoff et al., 2008; He et al., 2009).

Activation of integrin signaling by components of the extracellular matrix, such as FN, facilitates cytoskeletal reorganization before cell migration (Honda et al., 2009; Streuli and Akhtar, 2009; Vicente-Manzanares et al., 2009). FN regulates SMC migration in the ductus arteriosus, and this leads to the development of the intimal cushions, narrowing the ductal lumen and preparing the vessel for postnatal closure (Boudreau et al., 1991). Neural crest cells migrate along an FN gradient to form the cardiac outflow tracts and great vessels (Henderson et al., 2006; Eisenberg and Eisenberg, 2007). In coronary arteries after experimental heterotopic heart transplant, an FN gradient serves as a two-way highway to induce transendothelial T cell migration and to promote SMC migration in the neointima (Molossi et al., 1993, 1995). Also, after vascular injury and in association with PAH, accumulation of FN in the PA subendothelium may promote SMC migration (Mercurius and Morla, 1998; Morla and Mogford, 2000). Although our model supports a role for FN in promoting SMC migration but not proliferation, it is possible that, in disease, excessive production and accumulation of FN could also enhance the response of VSMCs to growth factors released after injury (Nelson et al., 1997; Raines et al., 2000).

FN is known to interact with the α4β1-, α5β1-, and $\alpha_v\beta3$-integrin complexes to promote SMC attachment, locomotion, and signal transduction (Jones et al., 1997; Barillari et al., 2001). We chose the FN CS-1 peptide to block FN–SMC interactions because it is more specific for FN than the RGD peptide, another inhibitory peptide. Also, this selects for the blockade of the α4β1-integrin complex, which is expressed on VSMCs (Duplàa et al., 1997; Waitkus-Edwards et al., 2002; Hsia et al., 2005). Our results are therefore in keeping with the specificity of the α4β1 complex in activating ILK-1 in our cells.

Our study demonstrates that the VSMC motility response to BMP-2 is dependent on the ability of ILK-1 to form and maintain a stable protein complex with Dvl. Formation of an ILK-1–Dvl complex was previously described in migrating metanephric mesenchymal cells in which significant colocalization of ILK-1 and Dvl in the cytoskeleton was related to formation of pseudopodia and filopodia (Torres and Nelson, 2000). These features are also observed with activation of the Wnt–PCP pathway (Simons and Mlodzik, 2008; de Jesus Perez et al., 2009). Thus, we propose that BMP-2 formation of functional ILK-1–Dvl complexes is required to trigger RhoA-Rac1 activation and coordinate the cytoskeletal changes necessary for hPASMC motility (Fig. 10 A).

Our study also shows that modulation of the Wnt–PCP pathway by BMP signaling is common to systemic as well as pulmonary VSMCs. Previous studies addressing the pathobiology of systemic vascular disease have suggested that coupling

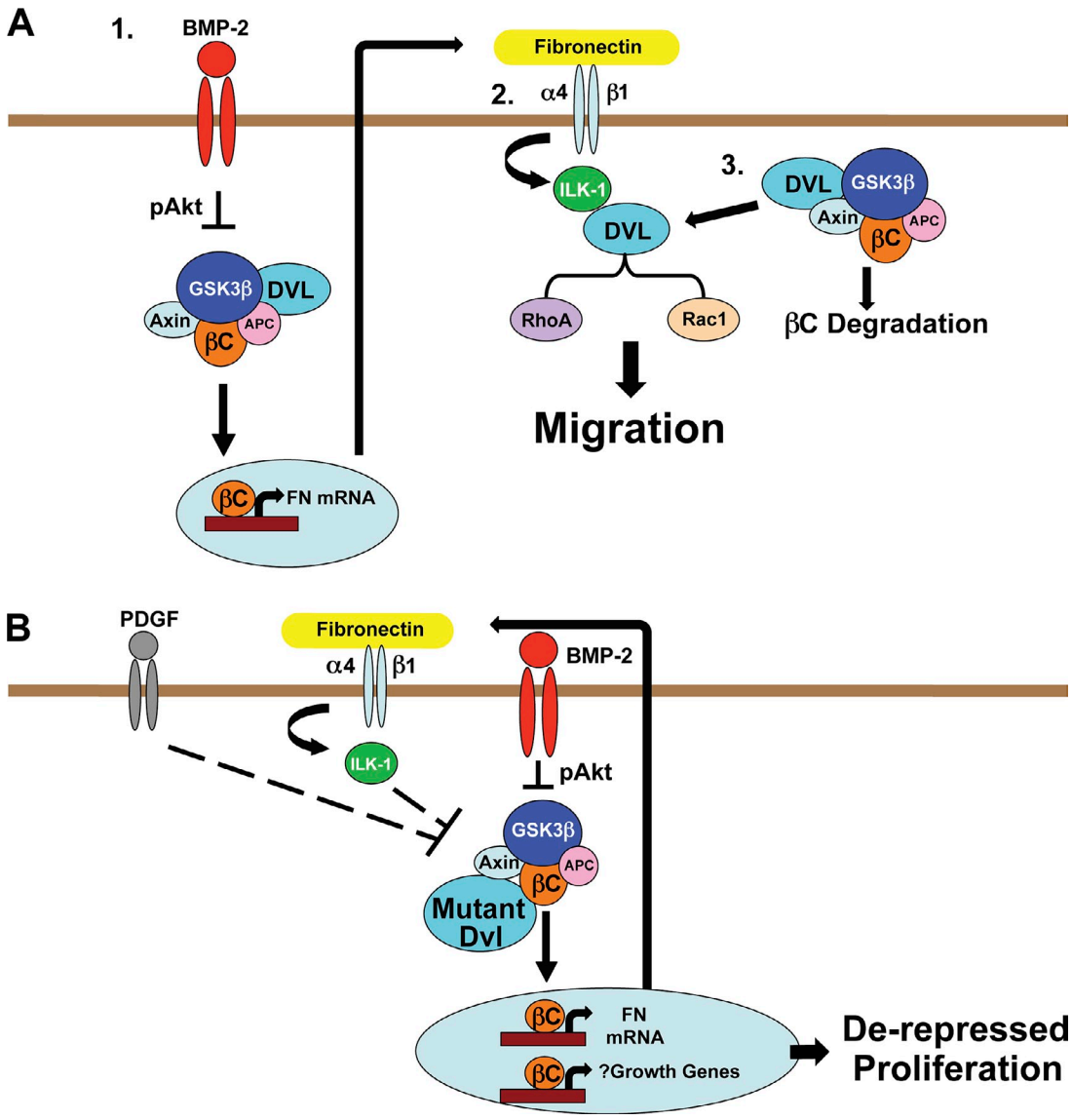

Figure 10. **Proposed models for BMP regulation of hPASMC motility and proliferation by recruitment of Wnt–βC and Wnt–PCP signaling.** (A) BMP-2 triggers βC accumulation via pAkt-mediated GSK3β inhibition followed by production and release of FN to the extracellular space (1). By binding to α4β1-integrin, FN activates ILK-1 and induces formation of a complex between ILK-1 and Dvl leading to RhoA and Rac1 activation (2) and simultaneous suppression of βC activation (3). (B) The inability to form or maintain a complex between ILK-1 and Dvl may facilitate hPASMC proliferation in response to growth factors such as PDGF-BB by enhancing βC signaling through ILK-1–mediated GSK3β inhibition. APC, adenomatous polyposis coli.

of VSMC motility and proliferation in response to growth factors such as PDGF-BB leads to adverse inward remodeling and the formation of a neointima (Fingerle et al., 1990; Reidy et al., 1992; Majack et al., 1996). Abrogating BMP-2–mediated motility with the mutant Dvl did not induce proliferation despite elevated βC levels. Rather the ability of BMP-2 to suppress PDGF-BB–mediated proliferation was abrogated, and the PDGF-BB–mediated proliferative response was enhanced. Collectively, this suggests that elevated levels of βC subvert the ability of BMP-2–mediated factors, such as ApoE, to inhibit PDGF-BB–mediated proliferation (Hansmann et al., 2007, 2008).

PDGF-BB can induce βC accumulation by disrupting the GSK3β–Axin–βC degradation complex via the p68 RNA helicase (Yang et al., 2006, 2007). Thus, suppressing βC can dampen SMC proliferation in response to PDGF-BB, and increasing βC can exaggerate the response, suggesting that this molecule acts in concert with other factors that are mediated by PDGF-BB. Therefore, it is possible to propose that, in the setting of vascular injury, the balance of growth (e.g., PDGF-BB) and anti-growth (e.g., BMP) factors released from the extracellular matrix (Ramirez et al., 2007; Ramirez and Sakai, 2010) in the vicinity of VSMCs serves to translocate cells to sites of injury to reinforce and repair the vessel wall while preventing the excessive proliferation, which would result in pathological remodeling.

We used the aortic stent as a way of testing whether, in the intact animal, the exaggerated increase in βC achieved with ΔDEP Dvl might result in heightened proliferation in response to a sustained injury and, thus, worsen neointima thickening. We were able to optimize transfection of the medial layer by first physically removing the intimal layer of the aortic grafts by

fitting a serrated catheter into the vascular lumen before sonoporation as described in Materials and methods. A limitation of our in vivo study is that we were not able, for technical reasons involved in embedding the stent, to perform immunohistochemistry on the sections. Thus, we are unable to show evidence of heightened βC signaling in the tissue. Moreover, because PDGF-BB stimulates motility by a non-Wnt–PCP-dependent mechanism, we could not completely dissociate the impact of motility from that of proliferation in this model.

Our study suggests that the propensity to develop systemic or pulmonary vascular disease may lie in gene variants that affect the function of molecules downstream of BMP–BMPRII to activate the Wnt–PCP pathway. It also suggests that activating this pathway could rescue loss of BMPRII function.

Materials and methods

Cell culture

Primary hPASMCs from large vessels and AoSMCs were obtained from three independent commercial sources (Lonza, Invitrogen, and Sciencell), and all cells were found to exhibit the same biological responses to BMP-2 stimulation. Cells were grown in SMC growth medium (5% FBS, 1 µg/ml hydrocortisone, 10 ng/ml of human epidermal growth factor, 3 ng/ml of basic fibroblast growth factor, 10 µg/ml heparin, 10 µg/ml gentamycin, and 0.25 µg/ml amphotericin), subcultured at a 1:4 ratio in 100-mm dishes (Corning), and used between passages 4 and 8. Cells were starved in SMC starvation medium (0.1% FBS and gentamycin/amphotericin) for 48 h before the experiment.

Proliferation and migration assays

Cells were seeded at 25 × 10^3 cells per well on 24-well plates in SMC growth medium and allowed to adhere overnight. The next day, cells were washed and incubated in SMC starvation medium for 48 h followed by stimulation with agonists for various time intervals indicated in the figure legends. Cells were then trypsinized and counted in a hemocytometer (de Jesus Perez et al., 2009). Migration assays were performed using the modified Boyden chamber assay: SMCs (10^4 cells/ml in 200 µl) were placed in the upper chamber in the absence or presence of 10 ng/ml BMP-2 (Sigma-Aldrich), 100 ng/ml Wnt3a (R&D Systems), or 20 ng/ml PDGF-BB (R&D Systems) in the lower chamber. Doses of these agonists were based on previous dose–response curves (Hansmann et al., 2008; de Jesus Perez et al., 2009; Spiekerkoetter et al., 2009). Similar responses with all three BMP ligands (BMP-2, BMP-4, and BMP-7) were observed in hPASMCs. In some motility experiments, the impact of different concentrations of the ROCK I/II–specific inhibitor Y-27632 (EMD) was measured against BMP-2. After 6 h of incubation, the cells were removed from the upper face of the membrane (Transwell), and those in the underside of the membrane were fixed and stained with 0.5% toluidine blue in 4% paraformaldehyde. Migration was quantified with an inverted phase-contrast microscope (Eclipse TS100/100-F; Nikon) by calculating the mean number of cells in six random 200× magnification fields per well. The migration index was obtained by comparing the values in the experimental groups with the unstimulated control. All assays were performed in triplicate, and three separate cell harvests were assessed.

RhoA and Rac1 pull-down assays

Cells were washed three times with ice-cold PBS. Lysates were prepared by adding 500 µl of ice-cold magnesium lysis buffer (10 mM Tris HCl, 1.0% SDS, and 0.2 mM PMSF) with protease and phosphatase inhibitor cocktails 1 and 2 (Sigma-Aldrich) and scraping into a 1.5-ml microcentrifuge tube before centrifugation at 14,000 rpm for 10 min.

Active forms of RhoA or Rac1 were precipitated using glutathione beads containing Rhotekin or PAK1, respectively, according to the manufacturer's instructions (Millipore). In brief, lysates were incubated with a slurry containing the glutathione beads for 1 h at 4°C with constant rotation. At the end of this period, beads were precipitated by centrifuging lysates at 14,000 *g* for 20 s. After washing three times with ice-cold buffer, beads were resuspended in Laemmli buffer, boiled, and then subjected to Western immunoblot analysis as described in Western immunoblotting. Levels of active RhoA and Rac1 were standardized against total RhoA and Rac1 in whole cell lysates (Ren and Schwartz, 2000).

Generation of the ΔPRS Dvl mutant

The insert containing the full-length sequence for WT Dvl was removed from the pCS2 vector backbone followed by purification from an agarose gel using the gel extraction kit (Purelink Quick Gel Extraction; Invitrogen). The insert was then ligated to the pALTER-MAX vector (Promega), and its presence was confirmed by DNA sequencing. A 500-bp region encompassing the PRS of Dvl (found between 1,050 and 1,100 bp of the Dvl nucleic acid sequence) was either maintained as WT or mutagenized to convert prolines to alanines (lowercase). 5′-CCGCGCACGGAGCCGGTGCGACCCATCGATCCCGGTGC-3′ was the native sequence and 5′-gCGCGCACGGAGgCGGTGCGACtCATCGtTgCCGaTGC-3′ was the mutant sequence. Site-directed mutagenesis was performed at Mutagenex Laboratories.

RNA interference

The siRNA duplexes (Thermo Fisher Scientific) specific for βC (ON-TARGETplus; GenBank/EMBL/DDBJ accession no. NM_001012329 and NM_020248; and CTNNB1 ID#S438; Applied Biosystems), ILK-1 (ON-TARGETplus; GenBank accession no. NM_001014794), and BMPRII (ON-TARGETplus; GenBank accession no. NM_001204) were transfected into VSMCs using nucleofection. Knockdown efficiency was evaluated 48 h later by measuring protein levels in lysates using a Western immunoblot (see Western immunoblotting).

Western immunoblotting

Samples were subjected to electrophoresis under reducing conditions and transferred to a polyvinylidene fluoride membrane, which was then blocked for 1 h in buffer (nonfat milk powder 5% in TBS/Tween 0.1%) and incubated with primary antibodies overnight at 4°C. Membranes were probed using antibodies for active βC, RhoA, and Rac1 (Millipore) and pSer 21 GSK3β (Cell Signaling Technology). Binding of secondary HRP antibodies was visualized by ECL or ECL plus (GE Healthcare). A loading control was evaluated by reprobing the membrane with a mouse monoclonal antibody to α-tubulin (Sigma-Aldrich).

For analysis of proteins secreted into cell media, cells were incubated in phenol-free DME (Invitrogen). After stimulation, the media were collected and transferred to centrifugal filter devices (Amicon Ultra-4; Millipore). After centrifugation, the protein concentration in the supernatant was measured using the Lowry assay before Western immunoblot analyses.

Densitometry of Western blots was performed via ImageJ (National Institutes of Health) as follows: all blots were first scanned using a photo scanner (Perfection 4490; Epson) at a resolution of 600 dots per inch and converted to TIF files. These files were then opened in ImageJ using the grayscale mode option available in the program. Once opened, all images were then inverted so that the dark parts of the film became light and the light parts turned dark. This was performed to increase the limit of detection of low intensity bands in the blots. Next, a rectangle was drawn around the highest expression band, and its mean density was measured using the measure function found in ImageJ. Once finished, the same rectangle was then used to measure all the bands within the blot. To control for the presence of artifacts in the blots, we drew the rectangle around the contours of the bands of interest and avoided including areas containing artifacts. Finally, the background density of the blot was measured using the same rectangle and subtracted from all the band measurements to give the net densitometry. The same procedure was then repeated with the corresponding loading controls.

Once the net densitometry values for experimental and loading controls were obtained, a ratio of experimental/loading control was calculated. The experimental/loading optical densitometry ratios (i.e., relative OD) of at least three independent replicates were then used to compare values across different experiments. Statistical analysis was performed using Prism software (4.0; GraphPad Software, Inc.).

Promoter–reporter assays, plasmids, and transfection methods

For measurements of βC-mediated changes in gene expression, we used the topflash/fopflash T cell factor/lymphoid enhancer factor reporter assay (Millipore). The topflash construct contains a promoter with eight T cell factor/LEF1–binding domains found in the promoters of βC target genes linked to a luciferase gene, whereas the fopflash construct has mutated binding sites and serves as a negative control. Cells were transfected with 2 µg of a plasmid in a transfection device (Nucleofector II Program A-033; Lonza) using the basic SMC Nucleofector kit (Lonza). After 24 h in starvation media, cells were stimulated with agonist, and luciferase production was measured 6 h later in a luminometer (Turner Biosystems) using the Dual-Luciferase Reporter Assay kit (Promega) according to the manufacturer's instructions. Renilla plasmid (Promega) cotransfection was used to control for transfection efficiency.

Plasmids encoding the GFP-tagged WT and ΔDEP form of Dvl cloned in pCS2 vectors were described previously (Axelrod et al., 1998). The plasmid containing the V5-tagged ILK-1 in a pcDNA3.1 vector was provided by S. Dedhar (University of British Columbia, Vancouver, British Columbia, Canada). A pcDNA 3 vector containing an Akt construct with a loss-of-function mutation in its active site (Akt1, K179M T308A S473A) was provided by W. Sellers (Dana-Farber Cancer Institute, Boston, MA).

Confocal microscopy

Cells were plated in four-chamber polystyrene glass slides (15×10^3 cells per chamber), starved for 48 h, and then stimulated with BMP-2 as specified. Cells were fixed in 4% paraformaldehyde and permeabilized with 0.1% Triton X-100 and 1% BSA in ice-cold PBS before overnight incubation with a primary antibody against V5 (Invitrogen) or FN (Sigma-Aldrich). The next day, samples were washed in PBS three times and incubated with either Alexa Fluor 488– or 555–tagged secondary antibodies (Invitrogen) for 1 h at room temperature. Before mounting, slides were treated with gold antifade solution containing DAPI (Invitrogen) and stored at 4°C until analysis.

Confocal analysis was performed using a confocal laser-scanning microscope (SP2 AOBS; Leica) using anHCX Plan Apochromat 63× NA 1.32–0.60 oil objective. Image acquisition was performed using the confocal software (v2.5, build 1347; Leica). Images were processed and saved in a JPEG format using Photoshop (Creative Suite 2; Adobe).

ILK-1 kinase assay

Cells were starved for 48 h before the experiment. After stimulation with agonist, cells were washed in PBS and lysed with ice-cold radio immunoprecipitation assay buffer (500 µl per T75 flask). Equivalent amounts (250 µg) of lysates were incubated overnight at 4°C with 3–5 ml of goat polyclonal anti-ILK1 antibody (Abcam). The next day, the immune complexes were precipitated with protein G–Sepharose 4 fast-flow beads (GE Healthcare) and washed three times with radio immunoprecipitation assay lysis buffer and three times with kinase buffer (50 mM Hepes, pH 7, 2 mM $MgCl_2$, 2 mM $MnCl_2$, 20 mM Na_3VO_4, and protease inhibitors). The kinase assay was performed using 2 µg GSK3β fusion protein (New England Biolabs, Inc.) as a substrate and 200 µM ATP in the reaction buffer (50 mM Hepes, pH 7, 2 mM $MgCl_2$, 2 mM $MnCl_2$, 20 mM Na_3VO_4, and 20 mM NaF) for 30 min at 30°C. Next, Laemmli buffer was added, and samples were boiled for 10 min before loading onto a 4–12% Bis-Tris SDS-PAGE gel. Phosphorylation of the substrate was detected by Western immunoblotting with anti-GSK3β Ser 21/9 antibody (Cell Signaling Technology; Delcommenne et al., 1998).

Digitally enhanced video differential interference contrast microscopy

48 h after transfection, cells were allowed to attach and spread on glass coverslips in the incubator and were then viewed using an inverted microscope (Axiovert 35; Carl Zeiss, Inc.) with a Plan Apochromat 100× oil immersion lens and a short-distance condenser. The microscope is also equipped with heated-stage differential interference contrast optics and epifluorescence. Filters and lightpaths were controlled with a filterwheel and shutters (Ludl Electronic Products Ltd.). For GFP visualization, a single-band excitation filter for FITC was used in combination with a beamsplitter and emission filter (Pinkel 1; Chroma Technology Corp.). Tissue-culture medium without phenol red was kept warm and buffered in a CO_2 incubator. The stage temperature was kept at 37°C with an automatic thermostat. Images were collected using a black and white charge-coupled device camera (C2400; Hamamatsu Photonics) with on-chip integration and a digital image processor (Argus 20; Hamamatsu Photonics). Acquired images were assembled in temporal sequences using Openlab software (PerkinElmer) and saved as QuickTime videos (Apple).

Co-IP

Analysis of protein–protein interactions was performed using a previously published protocol (Bonifacino et al., 2001). In brief, after stimulation, cells lysates were incubated with the immunoprecipitating antibody and with protein–Sepharose G beads. The samples were then subjected to Western immunoblot analysis.

Aortic stent graft procedure

Animal experiments were performed under a protocol approved by the Animal Care Committee at the Stanford University School of Medicine following the guidelines of the American Physiological Society. All mice were C57BL/6J (Jackson ImmunoResearch Laboratories, Inc.) between the ages of 8 and 12 wk. The operative procedure has been previously described (Ali et al., 2007) and involved grafting a thoracic aortic segment from a female donor mouse to the carotid artery of a male littermate recipient. To prevent thrombosis, mice received 10 mg/kg/d aspirin in the drinking water, beginning 1 wk before and continuing throughout the experimental period. In brief, all mice were anesthetized with 50 mg/kg of body weight of pentobarbital sodium (given intraperitoneally). The thoracic aorta of the donor female mouse was isolated from the arch to the diaphragm. A small transverse arteriotomy was made just superior to the diaphragmatic outlet. Before introduction of the stent, a serrated metal rod was introduced into the aorta lumen to remove the intimal layer. Next, a stainless-steel stent (Nanointerventions Ltd.) 2.5 × 0.6 mm in dimension was crimped onto a 1.25 × 13–mm balloon angioplasty catheter (Ivatec International) and guided retrograde to the midportion of the descending thoracic aorta, and the balloon was inflated to eight atmospheres of pressure for 30 s, deploying the stent to a final internal diameter of 1.25 mm (balloon/vessel ratio of 1.5:1). The stented aorta was harvested by sealing the intercostal branch vessels with electrocautery. After applying a proximal ligature, the stented aorta was filled endoluminally with 50 µl (i.e., 5 µg) of either GFP-tagged WT Dvl or ΔDEP Dvl plasmid and then sealed distally with a further ligature. The stented aortas containing endoluminal plasmid were sonoporated using a sonoporator (Sonidel P100; Sonidel Limited) following the manufacturer's instructions.

In the recipient (male) mouse, the right common carotid artery was isolated, ligated, and divided between ties at its midpoint. Polyethylene cuffs (0.65-mm diameter; Portex Ltd.) were placed over the ends of the vessel and anchored by microhemostatic clamps (Aesculap). Sutures at the ends of the artery were removed, and the artery was everted over the cuffs and secured with sutures. The stented aorta from the donor mouse was grafted by sleeving the ends of the aorta over the two ends of the carotid artery and ligating them. Vigorous pulsation in the conduit vessel confirmed successful engraftment.

Immunohistochemistry

Antigen retrieval was performed using the heat-mediated citrate buffer epitope retrieval method (10 mM sodium citrate and 0.05% Tween 20, pH 6.0). Staining was performed using the Vectastain Elite ABC kit (Vector Laboratories) according to the manufacturer's protocol. A primary rabbit anti-GFP antibody (Biodesign) was used to detect GFP or the plasmid distribution in the tissues.

OCT

OCT images were obtained with the OCT imaging system (M3; LightLab Imaging). ImageWire is an imaging probe that delivers the light to the tissue and collects the signals. The ImageWire consists of a 0.15-mm fiber-optic core inside a sheath with a maximum OD of 0.48 mm. Motorized pull-back OCT imaging was performed at a rate of 1.0 mm/s. Images were acquired at 15 frames per second, displayed with a color look-up table, and digitally archived. OCT measurements were performed using the LightLab OCT imaging proprietary software with a mouse-based interface. Lumen and stent cross-sectional areas (CSAs) were manually traced at 1.0-mm intervals. Intimal CSA was calculated as the stent CSA subtracted from the lumen CSA. The percentage of intimal area was calculated as intimal CSA divided by stent CSA. The mean percentage of intimal areas was calculated (Deuse et al., 2009).

Tissue preparation, histology, and lesion quantification

Vessels were harvested 21 d after surgery and fixed by perfusion in situ with 4% paraformaldehyde. Vessels were excised, fixed in paraformaldehyde overnight, and subsequently embedded in methyl methacrylate resin (Technovit 9100; TAAB Laboratories) according to the manufacturer's instructions. Four transverse sections were cut through each stent using a diamond-coated rotary saw (IsoMet 5000; Buehler) and polished (to 5–10 µm) using a polisher (Metaserv 2000; Buehler).

For histomorphometric analysis, sections were stained with hematoxylin and eosin. Lesions were quantified for total vessel area (area inside the external elastic lamina), neointimal area (area inside the internal elastic lamina minus stent struts and minus lumen), lumen, and stent expansion (area inside a polygon connecting the midpoint of each stent strut). Measurements of neointimal thickness were performed by measuring the perpendicular distance from lumen to internal elastic lamina at the midpoint between stent struts on each section (four to six measurements per section; four sections per vessel to generate $n = 1$). To label the nuclei, sections were depolymerized, and the tissue was treated with gold antifade solution containing DAPI and stored at 4°C until analysis.

Statistical analysis

The number of samples or animals studied per experiment is indicated in the figure legends. Values from multiple experiments are expressed as

means ± SEM. Statistical significance was determined using unpaired *t* test or one-way analysis of variance (ANOVA) followed by Dunnett's or Bonferroni's multiple comparison tests unless stated otherwise. A value of $P < 0.05$ was considered significant.

Online supplemental material

Fig. S1 shows that BMPRII knockdown reduces BMP-2–mediated motility and RhoA-Rac1 activation of hPASMCs transfected with either scrambled or BMPRII-specific siRNAs. Fig. S2 shows that the addition of wortmannin prevents BMP-2–mediated accumulation of βC and increase in transcriptional activity. Fig. S3 shows that BMP-2 can influence βC levels and stimulate motility in hAoSMCs. Videos 1 and 2 show WT Dvl-GFP–transfected hPASMCs in the absence and in the presence of BMP-2, respectively. Videos 3 and 4 show that, regardless of exposure to BMP-2, ΔDEP Dvl-GFP–transfected hPASMCs fail to redistribute GFP signals to the cell periphery, a finding that correlates with the lack of BMP-2–mediated cell motility. Online supplemental material is available at http://www.jcb.org/cgi/content/full/jcb.201008060/DC1.

We would like to express our gratitude to Dr. Michal Bental Roof and Karen D. Johnson for their invaluable help in the preparation of the figures for this manuscript, to Dr. Jeffrey Axelrod for his critical review of the manuscript, and to Michelle Fox, who helped us during the submission process.

This work was supported by an American Lung Association postdoctoral fellowship, a National Institutes of Health K12 award, and a Harold Amos Faculty Development Award to V.A. de Jesus Perez, National Institutes of Health grant R01HL074186 to M. Rabinovitch, and by an endowment of the Wall Center for Pulmonary Vascular Diseases at Stanford University. T.P. Alastalo was funded by postdoctoral fellowships from the Sigrid Juselius Foundation, the Instrumentarium Foundation, the Finnish Foundation for Cardiovascular Research, and the Academy of Finland.

Submitted: 10 August 2010
Accepted: 7 December 2010

References

Ali, Z.A., N.J. Alp, H. Lupton, N. Arnold, T. Bannister, Y. Hu, S. Mussa, M. Wheatcroft, D.R. Greaves, J. Gunn, and K.M. Channon. 2007. Increased in-stent stenosis in ApoE knockout mice: insights from a novel mouse model of balloon angioplasty and stenting. *Arterioscler. Thromb. Vasc. Biol.* 27:833–840. doi:10.1161/01.ATV.0000257135.39571.5b

Axelrod, J.D., J.R. Miller, J.M. Shulman, R.T. Moon, and N. Perrimon. 1998. Differential recruitment of Dishevelled provides signaling specificity in the planar cell polarity and Wingless signaling pathways. *Genes Dev.* 12:2610–2622. doi:10.1101/gad.12.16.2610

Barillari, G., L. Albonici, S. Incerpi, L. Bogetto, G. Pistritto, A. Volpi, B. Ensoli, and V. Manzari. 2001. Inflammatory cytokines stimulate vascular smooth muscle cells locomotion and growth by enhancing alpha-5beta1 integrin expression and function. *Atherosclerosis.* 154:377–385. doi:10.1016/S0021-9150(00)00506-2

Bonifacino, J.S., E.C. Dell'Angelica, and T.A. Springer. 2001. Immunoprecipitation. *Curr. Protoc. Immunol.* Chapter 8:Unit 8.3.

Boudreau, N., E. Turley, and M. Rabinovitch. 1991. Fibronectin, hyaluronan, and a hyaluronan binding protein contribute to increased ductus arteriosus smooth muscle cell migration. *Dev. Biol.* 143:235–247. doi:10.1016/0012-1606(91)90074-D

Boutros, M., N. Paricio, D.I. Strutt, and M. Mlodzik. 1998. Dishevelled activates JNK and discriminates between JNK pathways in planar polarity and wingless signaling. *Cell.* 94:109–118. doi:10.1016/S0092-8674(00)81226-X

Chait, A. 1987. Progression of atherosclerosis: the cell biology. *Eur. Heart J.* 8(Suppl. E):15–22.

Das, G., A. Jenny, T.J. Klein, S. Eaton, and M. Mlodzik. 2004. Diego interacts with Prickle and Strabismus/Van Gogh to localize planar cell polarity complexes. *Development.* 131:4467–4476. doi:10.1242/dev.01317

de Jesus Perez, V.A., T.P. Alastalo, J.C. Wu, J.D. Axelrod, J.P. Cooke, M. Amieva, and M. Rabinovitch. 2009. Bone morphogenetic protein 2 induces pulmonary angiogenesis via Wnt–β-catenin and Wnt–RhoA–Rac1 pathways. *J. Cell Biol.* 184:83–99. doi:10.1083/jcb.200806049

De Langhe, S.P., F.G. Sala, P.M. Del Moral, T.J. Fairbanks, K.M. Yamada, D. Warburton, R.C. Burns, and S. Bellusci. 2005. Dickkopf-1 (DKK1) reveals that fibronectin is a major target of Wnt signaling in branching morphogenesis of the mouse embryonic lung. *Dev. Biol.* 277:316–331. doi:10.1016/j.ydbio.2004.09.023

Delcommenne, M., C. Tan, V. Gray, L. Rue, J. Woodgett, and S. Dedhar. 1998. Phosphoinositide-3-OH kinase-dependent regulation of glycogen synthase kinase 3 and protein kinase B/AKT by the integrin-linked kinase. *Proc. Natl. Acad. Sci. USA.* 95:11211–11216. doi:10.1073/pnas.95.19.11211

Deuse, T., F. Ikeno, R.C. Robbins, and S. Schrepfer. 2009. Imaging in-stent restenosis: an inexpensive, reliable, and rapid preclinical model. *J. Vis. Exp.* (31):1346. doi:10.3791/1346

Ding, Q., W. Xia, J.C. Liu, J.Y. Yang, D.F. Lee, J. Xia, G. Bartholomeusz, Y. Li, Y. Pan, Z. Li, et al. 2005. Erk associates with and primes GSK-3beta for its inactivation resulting in upregulation of beta-catenin. *Mol. Cell.* 19:159–170. doi:10.1016/j.molcel.2005.06.009

Ding, V.W., R.H. Chen, and F. McCormick. 2000. Differential regulation of glycogen synthase kinase 3beta by insulin and Wnt signaling. *J. Biol. Chem.* 275:32475–32481. doi:10.1074/jbc.M005342200

Dobreva, I., A. Fielding, L.J. Foster, and S. Dedhar. 2008. Mapping the integrin-linked kinase interactome using SILAC. *J. Proteome Res.* 7:1740–1749. doi:10.1021/pr700852r

Duplàa, C., T. Couffinhal, P. Dufourcq, B. Llanas, C. Moreau, and J. Bonnet. 1997. The integrin very late antigen-4 is expressed in human smooth muscle cell. Involvement of alpha 4 and vascular cell adhesion molecule-1 during smooth muscle cell differentiation. *Circ. Res.* 80:159–169.

Dwivedi, A., G.B. Sala-Newby, and S.J. George. 2008. Regulation of cell-matrix contacts and beta-catenin signaling in VSMC by integrin-linked kinase: implications for intimal thickening. *Basic Res. Cardiol.* 103:244–256. doi:10.1007/s00395-007-0693-9

Eisenberg, L.M., and C.A. Eisenberg. 2007. Evaluating the role of Wnt signal transduction in promoting the development of the heart. *ScientificWorldJournal.* 7:161–176. doi:10.1100/tsw.2007.71

Feiguin, F., M. Hannus, M. Mlodzik, and S. Eaton. 2001. The ankyrin repeat protein Diego mediates Frizzled-dependent planar polarization. *Dev. Cell.* 1:93–101. doi:10.1016/S1534-5807(01)00010-7

Fingerle, J., Y.P. Au, A.W. Clowes, and M.A. Reidy. 1990. Intimal lesion formation in rat carotid arteries after endothelial denudation in absence of medial injury. *Arteriosclerosis.* 10:1082–1087.

Fukuda, T., K. Chen, X. Shi, and C. Wu. 2003. PINCH-1 is an obligate partner of integrin-linked kinase (ILK) functioning in cell shape modulation, motility, and survival. *J. Biol. Chem.* 278:51324–51333. doi:10.1074/jbc.M309122200

García, M.G., L.D. Alaniz, R.I. Cordo Russo, E. Alvarez, and S.E. Hajos. 2009. PI3K/Akt inhibition modulates multidrug resistance and activates NF-kappaB in murine lymphoma cell lines. *Leuk. Res.* 33:288–296. doi:10.1016/j.leukres.2008.06.010

Goodall, S., M. Crowther, D.M. Hemingway, P.R. Bell, and M.M. Thompson. 2001. Ubiquitous elevation of matrix metalloproteinase-2 expression in the vasculature of patients with abdominal aneurysms. *Circulation.* 104:304–309.

Hansmann, G., R.A. Wagner, S. Schellong, V.A. Perez, T. Urashima, L. Wang, A.Y. Sheikh, R.S. Suen, D.J. Stewart, and M. Rabinovitch. 2007. Pulmonary arterial hypertension is linked to insulin resistance and reversed by peroxisome proliferator-activated receptor-gamma activation. *Circulation.* 115:1275–1284.

Hansmann, G., V.A. de Jesus Perez, T.P. Alastalo, C.M. Alvira, C. Guignabert, J.M. Bekker, S. Schellong, T. Urashima, L. Wang, N.W. Morrell, and M. Rabinovitch. 2008. An antiproliferative BMP-2/PPARgamma/apoE axis in human and murine SMCs and its role in pulmonary hypertension. *J. Clin. Invest.* 118:1846–1857. doi:10.1172/JCI32503

He, W., C. Dai, Y. Li, G. Zeng, S.P. Monga, and Y. Liu. 2009. Wnt/beta-catenin signaling promotes renal interstitial fibrosis. *J. Am. Soc. Nephrol.* 20:765–776. doi:10.1681/ASN.2008060566

Henderson, D.J., H.M. Phillips, and B. Chaudhry. 2006. Vang-like 2 and noncanonical Wnt signaling in outflow tract development. *Trends Cardiovasc. Med.* 16:38–45. doi:10.1016/j.tcm.2005.11.005

Ho, B., and M.P. Bendeck. 2009. Integrin linked kinase (ILK) expression and function in vascular smooth muscle cells. *Cell Adh Migr.* 3:174–176. doi:10.4161/cam.3.2.7374

Honda, S., H. Shirotani-Ikejima, S. Tadokoro, Y. Maeda, T. Kinoshita, Y. Tomiyama, and T. Miyata. 2009. Integrin-linked kinase associated with integrin activation. *Blood.* 113:5304–5313. doi:10.1182/blood-2008-07-169136

Hsia, D.A., S.T. Lim, J.A. Bernard-Trifilo, S.K. Mitra, S. Tanaka, J. den Hertog, D.N. Streblow, D. Ilic, M.H. Ginsberg, and D.D. Schlaepfer. 2005. Integrin alpha4beta1 promotes focal adhesion kinase-independent cell motility via alpha4 cytoplasmic domain-specific activation of c-Src. *Mol. Cell. Biol.* 25:9700–9712. doi:10.1128/MCB.25.21.9700-9712.2005

Humbert, M., N.W. Morrell, S.L. Archer, K.R. Stenmark, M.R. MacLean, I.M. Lang, B.W. Christman, E.K. Weir, O. Eickelberg, N.F. Voelkel, and M. Rabinovitch. 2004. Cellular and molecular pathobiology of pulmonary arterial hypertension. *J. Am. Coll. Cardiol.* 43(Suppl 1):S13–S24. doi:10.1016/j.jacc.2004.02.029

Jones, P.L., J. Crack, and M. Rabinovitch. 1997. Regulation of tenascin-C, a vascular smooth muscle cell survival factor that interacts with the $\alpha_v \beta_3$ integrin to promote epidermal growth factor receptor phosphorylation and growth. *J. Cell Biol.* 139:279–293. doi:10.1083/jcb.139.1.279

Königshoff, M., N. Balsara, E.M. Pfaff, M. Kramer, I. Chrobak, W. Seeger, and O. Eickelberg. 2008. Functional Wnt signaling is increased in idiopathic pulmonary fibrosis. *PLoS One.* 3:e2142. doi:10.1371/journal.pone.0002142

Lee, K.S., H.J. Kim, Q.L. Li, X.Z. Chi, C. Ueta, T. Komori, J.M. Wozney, E.G. Kim, J.Y. Choi, H.M. Ryoo, and S.C. Bae. 2000. Runx2 is a common target of transforming growth factor beta1 and bone morphogenetic protein 2, and cooperation between Runx2 and Smad5 induces osteoblast-specific gene expression in the pluripotent mesenchymal precursor cell line C2C12. *Mol. Cell. Biol.* 20:8783–8792. doi:10.1128/MCB.20.23.8783-8792.2000

Legate, K.R., S.A. Wickström, and R. Fässler. 2009. Genetic and cell biological analysis of integrin outside-in signaling. *Genes Dev.* 23:397–418. doi:10.1101/gad.1758709

Leung, W.C., A. Lawrie, S. Demaries, H. Massaeli, A. Burry, S. Yablonsky, J.M. Sarjeant, E. Fera, E. Rassart, J.G. Pickering, and M. Rabinovitch. 2004. Apolipoprotein D and platelet-derived growth factor-BB synergism mediates vascular smooth muscle cell migration. *Circ. Res.* 95:179–186. doi:10.1161/01.RES.0000135482.74178.14

Logan, C.Y., and R. Nusse. 2004. The Wnt signaling pathway in development and disease. *Annu. Rev. Cell Dev. Biol.* 20:781–810. doi:10.1146/annurev.cellbio.20.010403.113126

Loirand, G., P. Guérin, and P. Pacaud. 2006. Rho kinases in cardiovascular physiology and pathophysiology. *Circ. Res.* 98:322–334. doi:10.1161/01.RES.0000201960.04223.3c

Machado, R.D., M.W. Pauciulo, J.R. Thomson, K.B. Lane, N.V. Morgan, L. Wheeler, J.A. Phillips III, J. Newman, D. Williams, N. Galiè, et al. 2001. BMPR2 haploinsufficiency as the inherited molecular mechanism for primary pulmonary hypertension. *Am. J. Hum. Genet.* 68:92–102. doi:10.1086/316947

Majack, R.A., N.A. Grieshaber, C.L. Cook, M.C. Weiser, R.C. McFall, S.S. Grieshaber, M.A. Reidy, and C.F. Reilly. 1996. Smooth muscle cells isolated from the neointima after vascular injury exhibit altered responses to platelet-derived growth factor and other stimuli. *J. Cell. Physiol.* 167:106–112. doi:10.1002/(SICI)1097-4652(199604)167:1<106::AID-JCP12>3.0.CO;2-9

Mercurius, K.O., and A.O. Morla. 1998. Inhibition of vascular smooth muscle cell growth by inhibition of fibronectin matrix assembly. *Circ. Res.* 82:548–556.

Molossi, S., N. Clausell, and M. Rabinovitch. 1993. Coronary artery endothelial interleukin-1 beta mediates enhanced fibronectin production related to post-cardiac transplant arteriopathy in piglets. *Circulation.* 88:II248–II256.

Molossi, S., M. Elices, T. Arrhenius, R. Diaz, C. Coulber, and M. Rabinovitch. 1995. Blockade of very late antigen-4 integrin binding to fibronectin with connecting segment-1 peptide reduces accelerated coronary arteriopathy in rabbit cardiac allografts. *J. Clin. Invest.* 95:2601–2610. doi:10.1172/JCI117962

Morla, A.O., and J.E. Mogford. 2000. Control of smooth muscle cell proliferation and phenotype by integrin signaling through focal adhesion kinase. *Biochem. Biophys. Res. Commun.* 272:298–302. doi:10.1006/bbrc.2000.2769

Morrell, N.W. 2006. Pulmonary hypertension due to BMPR2 mutation: a new paradigm for tissue remodeling? *Proc. Am. Thorac. Soc.* 3:680–686. doi:10.1513/pats.200605-118SF

Morrell, N.W., X. Yang, P.D. Upton, K.B. Jourdan, N. Morgan, K.K. Sheares, and R.C. Trembath. 2001. Altered growth responses of pulmonary artery smooth muscle cells from patients with primary pulmonary hypertension to transforming growth factor-beta(1) and bone morphogenetic proteins. *Circulation.* 104:790–795. doi:10.1161/hc3201.094152

Nakaoka, T., K. Gonda, T. Ogita, Y. Otawara-Hamamoto, F. Okabe, Y. Kira, K. Harii, K. Miyazono, Y. Takuwa, and T. Fujita. 1997. Inhibition of rat vascular smooth muscle proliferation in vitro and in vivo by bone morphogenetic protein-2. *J. Clin. Invest.* 100:2824–2832. doi:10.1172/JCI119830

Nelson, P.R., S. Yamamura, and K.C. Kent. 1997. Platelet-derived growth factor and extracellular matrix proteins provide a synergistic stimulus for human vascular smooth muscle cell migration. *J. Vasc. Surg.* 26:104–112. doi:10.1016/S0741-5214(97)70153-8

Ng, S.S., T. Mahmoudi, E. Danenberg, I. Bejaoui, W. de Lau, H.C. Korswagen, M. Schutte, and H. Clevers. 2009. Phosphatidylinositol 3-kinase signaling does not activate the wnt cascade. *J. Biol. Chem.* 284:35308–35313. doi:10.1074/jbc.M109.078261

Penton, A., A. Wodarz, and R. Nusse. 2002. A mutational analysis of dishevelled in *Drosophila* defines novel domains in the dishevelled protein as well as novel suppressing alleles of axin. *Genetics.* 161:747–762.

Picard, M., R.J. Petrie, J. Antoine-Bertrand, E. Saint-Cyr-Proulx, J.F. Villemure, and N. Lamarche-Vane. 2009. Spatial and temporal activation of the small GTPases RhoA and Rac1 by the netrin-1 receptor UNC5a during neurite outgrowth. *Cell. Signal.* 21:1961–1973. doi:10.1016/j.cellsig.2009.09.004

Rader, K., R.A. Orlando, X. Lou, and M.G. Farquhar. 2000. Characterization of ANKRA, a novel ankyrin repeat protein that interacts with the cytoplasmic domain of megalin. *J. Am. Soc. Nephrol.* 11:2167–2178.

Raines, E.W., and R. Ross. 1993. Smooth muscle cells and the pathogenesis of the lesions of atherosclerosis. *Br. Heart J.* 69(Suppl.):S30–S37. doi:10.1136/hrt.69.1_Suppl.S30

Raines, E.W., H. Koyama, and N.O. Carragher. 2000. The extracellular matrix dynamically regulates smooth muscle cell responsiveness to PDGF. *Ann. NY Acad. Sci.* 902:39–52. doi:10.1111/j.1749-6632.2000.tb06299.x

Ramirez, F., and L.Y. Sakai. 2010. Biogenesis and function of fibrillin assemblies. *Cell Tissue Res.* 339:71–82. doi:10.1007/s00441-009-0822-x

Ramirez, F., L.Y. Sakai, D.B. Rifkin, and H.C. Dietz. 2007. Extracellular microfibrils in development and disease. *Cell. Mol. Life Sci.* 64:2437–2446. doi:10.1007/s00018-007-7166-z

Reidy, M.A., J. Fingerle, and V. Lindner. 1992. Factors controlling the development of arterial lesions after injury. *Circulation.* 86(6 Suppl.):III43–III46.

Ren, X.D., and M.A. Schwartz. 2000. Determination of GTP loading on Rho. *Methods Enzymol.* 325:264–272. doi:10.1016/S0076-6879(00)25448-7

Sarjeant, J.M., A. Lawrie, C. Kinnear, S. Yablonsky, W. Leung, H. Massaeli, W. Prichett, J.P. Veinot, E. Rassart, and M. Rabinovitch. 2003. Apolipoprotein D inhibits platelet-derived growth factor-BB-induced vascular smooth muscle cell proliferated by preventing translocation of phosphorylated extracellular signal regulated kinase 1/2 to the nucleus. *Arterioscler. Thromb. Vasc. Biol.* 23:2172–2177. doi:10.1161/01.ATV.0000100404.05459.39

Sedding, D.G., J. Hermsen, U. Seay, O. Eickelberg, W. Kummer, C. Schwencke, R.H. Strasser, H. Tillmanns, and R.C. Braun-Dullaeus. 2005. Caveolin-1 facilitates mechanosensitive protein kinase B (Akt) signaling in vitro and in vivo. *Circ. Res.* 96:635–642. doi:10.1161/01.RES.0000160610.61306.0f

Simons, M., and M. Mlodzik. 2008. Planar cell polarity signaling: from fly development to human disease. *Annu. Rev. Genet.* 42:517–540. doi:10.1146/annurev.genet.42.110807.091432

Spiekerkoetter, E., C. Guignabert, V. de Jesus Perez, T.P. Alastalo, J.M. Powers, L. Wang, A. Lawrie, N. Ambartsumian, A.M. Schmidt, M. Berryman, et al. 2009. S100A4 and bone morphogenetic protein-2 codependently induce vascular smooth muscle cell migration via phospho-extracellular signal-regulated kinase and chloride intracellular channel 4. *Circ. Res.* 105:639–647. doi:10.1161/CIRCRESAHA.109.205120

Streuli, C.H., and N. Akhtar. 2009. Signal co-operation between integrins and other receptor systems. *Biochem. J.* 418:491–506. doi:10.1042/BJ20081948

Thompson, K., and M. Rabinovitch. 1996. Exogenous leukocyte and endogenous elastases can mediate mitogenic activity in pulmonary artery smooth muscle cells by release of extracellular-matrix bound basic fibroblast growth factor. *J. Cell Physiol.* 166:495–505.

Thornton, T.M., G. Pedraza-Alva, B. Deng, C.D. Wood, A. Aronshtam, J.L. Clements, G. Sabio, R.J. Davis, D.E. Matthews, B. Doble, and M. Rincon. 2008. Phosphorylation by p38 MAPK as an alternative pathway for GSK3beta inactivation. *Science.* 320:667–670. doi:10.1126/science.1156037

Torres, M.A., and W.J. Nelson. 2000. Colocalization and redistribution of dishevelled and actin during Wnt-induced mesenchymal morphogenesis. *J. Cell Biol.* 149:1433–1442. doi:10.1083/jcb.149.7.1433

Troussard, A.A., C. Tan, T.N. Yoganathan, and S. Dedhar. 1999. Cell-extracellular matrix interactions stimulate the AP-1 transcription factor in an integrin-linked kinase- and glycogen synthase kinase 3-dependent manner. *Mol. Cell. Biol.* 19:7420–7427.

Velyvis, A., Y. Yang, C. Wu, and J. Qin. 2001. Solution structure of the focal adhesion adaptor PINCH LIM1 domain and characterization of its interaction with the integrin-linked kinase ankyrin repeat domain. *J. Biol. Chem.* 276:4932–4939. doi:10.1074/jbc.M007632200

Vicente-Manzanares, M., C.K. Choi, and A.R. Horwitz. 2009. Integrins in cell migration—the actin connection. *J. Cell Sci.* 122:199–206. doi:10.1242/jcs.018564

Voelkel, N.F., and R.M. Tuder. 1997. Cellular and molecular biology of vascular smooth muscle cells in pulmonary hypertension. *Pulm. Pharmacol. Ther.* 10:231–241. doi:10.1006/pupt.1998.0100

Waitkus-Edwards, K.R., L.A. Martinez-Lemus, X. Wu, J.P. Trzeciakowski, M.J. Davis, G.E. Davis, and G.A. Meininger. 2002. alpha(4)beta(1) Integrin activation of L-type calcium channels in vascular smooth muscle causes arteriole vasoconstriction. *Circ. Res.* 90:473–480. doi:10.1161/hh0402.105899

Wertz, J.W., and P.M. Bauer. 2008. Caveolin-1 regulates BMPRII localization and signaling in vascular smooth muscle cells. *Biochem. Biophys. Res. Commun.* 375:557–561. doi:10.1016/j.bbrc.2008.08.066

Willette, R.N., J.L. Gu, P.G. Lysko, K.M. Anderson, H. Minehart, and T. Yue. 1999. BMP-2 gene expression and effects on human vascular smooth muscle cells. *J. Vasc. Res.* 36:120–125. doi:10.1159/000025634

Willis, A.I., D. Pierre-Paul, B.E. Sumpio, and V. Gahtan. 2004. Vascular smooth muscle cell migration: current research and clinical implications. *Vasc. Endovascular Surg.* 38:11–23. doi:10.1177/153857440403800102

Yang, L., C. Lin, and Z.R. Liu. 2006. P68 RNA helicase mediates PDGF-induced epithelial mesenchymal transition by displacing Axin from beta-catenin. *Cell.* 127:139–155. doi:10.1016/j.cell.2006.08.036

Yang, L., C. Lin, S. Zhao, H. Wang, and Z.R. Liu. 2007. Phosphorylation of p68 RNA helicase plays a role in platelet-derived growth factor-induced cell proliferation by up-regulating cyclin D1 and c-Myc expression. *J. Biol. Chem.* 282:16811–16819. doi:10.1074/jbc.M610488200

Zhang, S., I. Fantozzi, D.D. Tigno, E.S. Yi, O. Platoshyn, P.A. Thistlethwaite, J.M. Kriett, G. Yung, L.J. Rubin, and J.X. Yuan. 2003. Bone morphogenetic proteins induce apoptosis in human pulmonary vascular smooth muscle cells. *Am. J. Physiol. Lung Cell. Mol. Physiol.* 285:L740–L754.

Zhang, Y., K. Chen, L. Guo, and C. Wu. 2002. Characterization of PINCH-2, a new focal adhesion protein that regulates the PINCH-1-ILK interaction, cell spreading, and migration. *J. Biol. Chem.* 277:38328–38338. doi:10.1074/jbc.M205576200